CHARACTERIZATION OF SURFACTANT DISPERSED SINGLE WALL NANOTUBE - POLYSTYRENE MATRIX COMPOSITE

A Thesis

by

DANIEL OSAGIE OYINKURO AYEWAH

Submitted to the Office of Graduate Studies of
Texas A&M University
in partial fulfillment of the requirements for the degree of

MASTER OF SCIENCE

August 2007

Major Subject: Aerospace Engineering

CHARACTERIZATION OF SURFACTANT DISPERSED SINGLE WALL NANOTUBE - POLYSTYRENE MATRIX COMPOSITE

A Thesis

by

DANIEL OSAGIE OYINKURO AYEWAH

Submitted to the Office of Graduate Studies of
Texas A&M University
in partial fulfillment of the requirements for the degree of

MASTER OF SCIENCE

Approved by:

Chair of Committee,	Dimitris C. Lagoudas
Committee Members,	Daniel C. Davis
	Hung-Jue Sue
Head of Department,	Helen Reed

August 2007

Major Subject: Aerospace Engineering

ABSTRACT

Characterization of Surfactant Dispersed Single Wall Nanotube - Polystyrene Matrix Nanocomposite. (August 2007)

Daniel Osagie Oyinkuro Ayewah, B.S., Texas A&M University

Chair of Advisory Committee: Dr. Dimitris Lagoudas

Carbon nanotubes (CNT) are a new form of carbon with exceptional electrical and mechanical properties. This makes them attractive as inclusions in nanocomposite materials with the potential to provide improvements in electrical and mechanical properties and allows for the creation of a new range of multifunctional materials. In this study single wall carbon nanotubes (SWCNT) were dispersed in polystyrene using a solution mixing method, with the aid of a surfactant. A good dispersion was achieved and the resulting nanocomposites were characterized for electrical conductivity and mechanical properties by 3 point flexural and fracture toughness tests.

Results show a significant improvement in electrical properties with electrical percolation occurring between 0.1 and 0.2 wt%. A minor improvement was observed in the flexural modulus but the strength and fracture toughness values in the nanocomposites decreased relative to the neat material. Scanning electron microscopy (SEM) was performed to characterize the morphology and fracture surface of the specimens. The results of testing and microscopy show that the presence of the

nanotubes has an adverse effect on the crazing mechanism in Polystyrene (PS) resulting in a deterioration of the mechanical properties that depend on this mechanism.

ACKNOWLEDGEMENTS

I would like to thank my committee chair, Dr. Dimitris Lagoudas, and committee members, Dr. Daniel Davis and Dr. Hung-Jue Sue, for their guidance during the course of my studies. Special thanks to Dr. Davis for his guidance in the day to day activities of the research.

I would also like to thank Dr. Krishnamoorti and the members of his research group at the University of Houston for the opportunity to collaborate with them in characterizing material developed in their labs.

Finally I would like to thank my fellow students, friends and family for all their support during the course of my studies here at Texas A&M University.

NOMENCLATURE

ASTM	American Society for Testing and Materials
CNT	Carbon Nanotubes
CVD	Chemical Vapor Deposition
DMA	Dynamic Mechanical Analysis
EMI	Electromagnetic Interference
MWCNT	Multi-Wall Carbon Nanotubes
OM	Optical Microscopy
PS	Polystyrene
PS-SWCNT	Polystyrene – Single Wall Carbon Nanotube nanocomposite
SEM	Scanning Electron Microscopy
SENB	Single Edge Notch Bend
SWCNT	Single Wall Carbon Nanotubes
TEM	Transmission Electron Microscopy

TABLE OF CONTENTS

Page

LIST OF TABLES

Page

LIST OF FIGURES

Page

Page

CHAPTER I

INTRODUCTION

Composite materials have been in commercial production for many years. They are made by the integration of two or more materials, arranged in an optimal fashion, to take advantage of the best properties of each material and engineer an improved material. Common examples include carbon fiber and glass fiber embedded in a polymer matrix. Their properties can be tailored to specific applications by controlling the quantity and structure of their constituent materials. Composites therefore provide enhanced properties as well as the flexibility to tailor their properties.

Nanocomposites are a more recent special class of composite materials having inclusions with dimensions on the order of 0.1 – 100nm[1]. They may be grouped into three categories based on the nature of their inclusions: particles, layered materials and fibrous materials[1]. Carbon nanotubes fall into the fibrous materials category since they have an aspect ratio on the order of 1000.

This thesis follows the style of the Journal of Applied Polymer Science.

The relatively recent discovery of carbon nanotubes (CNT)[2] has stimulated a wide range of research activity in the field of materials science due to their reported exceptional properties and the potential to harness these properties in composite materials. CNTs exist as single wall (SWCNT), double wall (DWCNT) or multi-wall (MWCNT) structures. SWCNT theoretically exhibit the best mechanical and electrical properties but because SWCNTs are more expensive to process, they are found in fewer studies in literature. The structure of a single wall carbon nanotube (SWCNT) is like a single layer of graphite rolled into a tube with a diameter on the order of $1\,nm$ and length on the order of $1\,\mu m$. Their mechanical and electrical properties make them excellent candidates as fillers in polymeric materials resulting in new multifunctional materials. We define a multifunctional material as one that has mechanical properties and at least one other property of interest in a particular application; for example electrical, thermal or gas barrier properties. These properties allow the material to serve multiple functions simultaneously in their applications. The resulting nanocomposites have high expectations as revolutionary materials due not only to their enhanced properties but also due to the ability to tailor these properties by controlling the amount and type of nanotubes they contain. Despite the exceptional properties of the nanotube it is very important (as with any composite system) to understand the interaction between the filler material and the polymer matrix in order to be able to engineer a system with the desired improved properties. Possible applications of nanocomposites containing SWCNT are:

- Structural Reinforcement: Nanotubes can act as structural reinforcement in polymers and improve mechanical properties such as stiffness strength and

fracture toughness. They can also act as an additional structural reinforcement in the matrix of a carbon fiber composite material.

- Electromagnetic Interference (EMI) Shielding: This is important in the world of electronics. Electrical circuits emit electromagnetic (EM) waves and are affected by external sources of electromagnetic waves. Conductive materials used to package electronics have the ability to shield EMI thereby containing emission from internal circuits while shielding from external sources of EMI as well.
- Electrostatic Discharge: Conductive materials allow current to flow through them which prevents the build up of static charge and eliminates the risk of sparks in a flammable environment.
- Electrostatic Painting: This method of painting involves charging the paint nozzle and the part to be painted at opposite charges such that paint particles are immediately attracted to the part. It is an efficient way of painting currently in use for metal parts in the automotive industry for example[3]. Its use may be extended to plastic surfaces such as car bumpers if they are made conductive. Adding CNTs to polymers in the right quantities may result in a material with a degree of conductivity that is sufficient to allow electrostatic painting.

In a previous study[4] good dispersion was achieved using a non-covalent functionalization method to disperse SWCNTs. This method involves the use of a surfactant to aid dispersion by sonication in a solvent before incorporation in a polymer. A similar dispersion method is used in this study to disperse SWCNT in polystyrene.

The resulting polystyrene nanocomposite (PS-SWCNT) material was characterized to determine its electrical and mechanical properties. OM and SEM were used to study how the properties relate to changes in the morphology of the material with the addition of nanotubes.

CHAPTER II

LITERATURE REVIEW

2.1 Carbon Nanotubes

Carbon nanotubes are reported to have an elastic modulus comparable to that of diamond (1.2 TPa) and a strength 10 – 100 times that of high strength steel[5]. Their mechanical properties may be attributed to the strength of the carbon-carbon covalent bond (also observed in diamond) that makes up their structure. CNTs can be either metallic or semi-conducting depending on their chirality which may be loosely described as the orientation of the graphene lattice relative to the CNT axis. Statistically one third of the nanotubes in a batch are metallic[6]. Metallic CNTs are highly conductive. It is estimated that they can carry a current of $1\times10^{9} amp/cm^{2}$ while copper wires burn out at about $1\times10^{6} amp/cm^{2}$ [1].

Fabrication methods for nanotubes include chemical vapor deposition (CVD), arc discharge, laser ablation and gas phase catalytic growth from carbon monoxide[5]. The nanotubes used in this study are fabricated by the HiPco process: a gas phase catalytic growth method in which carbon monoxide flows over catalytic clusters of iron at high pressure (30 – 50atm) and temperature (900 – 1100°C)[7].

2.2 Polystyrene

Polystyrene (PS) is a well characterized and widely studied polymer[8,9]. It is considered a commodity plastic having a wide range of commercial applications today. These range from making light switches for the home to the external shell of televisions, computers and other appliances used on a daily basis. Because of its popularity and widespread use it is an obvious candidate for nanocomposite research to enhance its properties and broaden the scope of its applications. It is also relatively cheap and easy to process and manufacture.

2.2.1 Chemical Structure

Polystyrene has a chemical structure similar to that of polyethylene except that one hydrogen location in the ethylene monomer is replaced by a benzene ring giving the styrene monomer. The polymer chain can exist in isotactic, atactic and syndiotactic configurations (Figure 1), each with different physical and chemical characteristics. Most commercially available ‘general purpose’ PS today is atactic i.e. the location of the benzene ring occurs in a random manner along the backbone. This lack of order in the structure prevents any kind of crystallization from taking place as it does in syndiotactic and isotactic PS. Atactic PS is therefore amorphous and hence transparent. It has a glass transition temperature of about 100°C and exists in the glassy state at room temperature. Although it is considered a brittle polymer is can sustain some yielding by crazing.

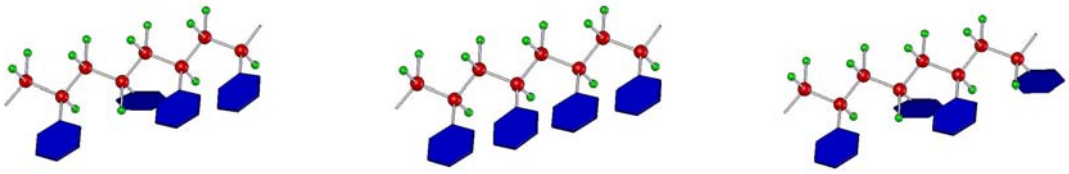

(a) (b) (c)

Figure 1 Configurations of polystyrene. (a) atactic polystyrene has a random placement of the benzene ring (b) isotactic polystyrene has a constant placement of the benzene ring (c) syndiotactic polystyrene has an alternating placement of the benzene ring.

2.2.2 Toughness

Toughness is the ability of a material to resist brittle failure in the presence of a sharp crack. This is achieved through a variety of energy absorbing mechanisms that vary depending on the material system. Toughening mechanisms include shear banding, crazing, microcracking, crack bridging, crack bifurcation, cavitation and crack pinning. These mechanisms all have the same effect of slowing down or even stopping a sharp crack from propagating. As filler materials, nano particles have the potential to enhance existing toughening mechanisms or introduce new ones that are a result of their interaction with the polymer matrix. In a successful system, the result is a durable material able to withstand structural abuse without suddenly failing. Advanced engineering applications are driving the improvement of toughness and durability of polymer systems today.

2.2.3 Natural Toughening Mechanisms of PS

The predominant natural toughening mechanism in PS and other glassy polymers is crazing. Crazing occurs at the onset of yielding under conditions of maximum normal stress. It is a normal (as opposed to shear) yielding mechanism that differs from a crack by the presence of many polymer fibrils connecting the two faces of the crack. The fibrils have an average diameter of 6 – 9nm and the craze band has a volume fraction of 0.25[10] i.e. 25% of the craze band consists of polymer fibrils. In the process of yielding, multiple crazes form across the sample in a plane perpendicular to the direction of load application. The ultimate failure occurs when one of the craze bands breaks down by molecular disentanglement of the fibrils. Crazing absorbs energy and widespread stable crazing can have a strong toughening effect on a polymer[11].

2.3 Polystyrene Nanocomposites

Research into polymer nanocomposites aims at producing novel materials with increased stiffness, strength and toughness, while introducing other properties such as electrical conductivity[12]. Nanocomposites are highly effective at low volume fractions because of their high surface area to volume ratio at the nano scale. The large surface area allows for extensive interaction with the matrix material[13].

This section reviews previous work done specifically on polystyrene nanocomposites. Factors such as dispersion, the nature of the CNTs, and their interaction with the matrix material affect the reinforcing ability of the nanotubes. The resulting material properties are described.

2.3.1 Mechanical Properties

This section reviews papers focusing on methods employed to improve the stiffness, strength and toughness of polymers by the addition of nanofillers.

Thostenson et al.[14] describe a system in which CVD grown MWCNT are dispersed in a PS matrix at 5wt% by a high shear mixing of the melt in a micro-scale twin screw extruder. The melt is then drawn to induce a preferential alignment of the nanotubes. Thin film samples of the neat material and the nanocomposite are made with one set drawn to induce preferential alignment and another set molded in a hot press resulting in random orientation. Static tensile tests and DMA are performed to study the effects of preferential alignment and the presence of nanotubes on the mechanical properties of the material. The results show a significant increase in the elastic modulus of the aligned nano-composite; an improvement which is five times greater than the improvement for the randomly oriented nanocomposite. The change in elastic modulus between the drawn and un-drawn neat PS was not statistically significant indicating that the large improvement in modulus of the nanocomposite was due to the nanotube orientation and not the polymer chain orientation. TEM images of a crack interacting with the nanotubes show a crack bridging mechanism as well as fractured tubes with matrix material still adhered to them indicating good wetting and adhesion of the nanotubes to the matrix. The material also showed a marked improvement in yield and ultimate strength which was attributed to a good load transfer between the polymer and the nanotubes. It is interesting to note that although the ultimate strength of the aligned nanocomposite is higher than that of the neat drawn PS it supports substantially less

yielding than the neat material indicating that the nanotubes may decrease the amount of yielding in PS.

In another study D.Qian et al.[15] describe a system consisting of CVD grown MWCNT in a polystyrene matrix. Dispersion is achieved here by dissolving the PS and the CNT separately in toluene. The CNT is dispersed in toluene by sonication. After dispersion the PS-toluene solution and the MWCNT-toluene suspension are mixed in a bath sonicator for 30 minutes to 1hr and then cast into a culture dish. The toluene evaporates resulting in a nano-composite film about 0.4mm thick. Samples with $15\mu m$ and $50\mu m$ average length MWCNT (30nm diameter) at 1wt% loading, are studied and compared to neat PS. Tensile test results show a 25% increase in the failure strength for both samples. The elastic modulus increases by 35% and 42% for the $15\mu m$ and $50\mu m$ samples respectively indicating that the elastic modulus is affected by the length of the nanotubes while the strength is not. This is understandable since the load transfer may be expected to be more effective with longer tubes. TEM images show evidence of crack bridging and nanotube breakage at a crack in the nano-composite film.

In summary improvements in stiffness can be achieved through ensuring a good interfacial interaction between the nano-inclusion and the matrix. This enhances the efficiency of load transfer to the reinforcing inclusion. Alignment of high aspect ratio inclusions[14] in the direction of the applied load is a very effective way of improving stiffness because the inclusions are oriented in the direction in which they are stiffest.

2.3.2 Electrical Properties

A major benefit of using carbon nanotubes to make composite materials is their ability to introduce electrical properties to the polymer. The result is a conductive plastic useful for applications like electrostatic discharge and electromagnetic induction (EMI) shielding materials. Once one succeeds in achieving enhanced mechanical properties in a nanocomposite with a high enough loading of CNT the new material will possess both enhanced mechanical properties and a new property, electrical conductivity, which makes it a multifunctional material. Nanotubes make polymers conductive by forming a continuous path in the polymer through which electrons can pass. As the loading of nanotubes increases, proximity of individual tubes and bundles decreases until they are close enough to form a continuous path for conduction. Studies[12] indicate that the flow of elections may be facilitated not only by direct contact of the nanotubes in these networks but also by an electron tunneling mechanism between nanotubes in close proximity. Percolation theory predicts that there is a critical loading of nanotubes that forms this continuous network[12] and converts the material from an insulator to a conductor.

Percolation has been observed to occur at SWCNT loadings as low as 0.05wt% in a polystyrene[16] and polyimide[12] system. Such low percolation is a result of effective dispersion. Dispersion aims at breaking up SWCNT bundles to smaller sizes which maximizes their aspect ratio and increases the probability of formation of a conductive network in the polymer at lower loadings of SWCNT. Measuring electrical conductivity therefore can also be used to study the quality of dispersion in a CNT nanocomposite.

CHAPTER III

MATERIAL SYSTEM AND FABRICATION

The polystyrene used in this study has an atactic configuration hence it is amorphous and colorless. It has a molecular weight M_w of about 280000. The SWNT were made by the HiPco process[7] and used in the as made unpurified state.

3.1 Solution mixing of SWNT in PS

The SWNTs are incorporated into the PS polymer by a solution mixing technique[4]. Polystyrene is dissolved into Toluene to form a polymer solution. SWCNTs and Cetyl Trimethyl Ammonium Bromide (CTAB) surfactant from Sigma-Aldrich are sonicated together in toluene for 2 hours to disperse the SWCNTs using a Fischer Scientific ultrasonic bath at 44 kHz frequency. The dispersion is then mixed with the PS solution using a stirrer. The composite is finally precipitated from solution by adding cold methanol. The resulting nanocomposite is annealed at $170°C$ under vacuum for 24 hours and then allowed to cool slowly to room temperature while still under a vacuum.

3.2 Specimen Fabrication

In this study five different samples are studied; neat, 0.1, 0.2, 0.3, and 1wt% PS-SWNT. In order to carry out tests on this material it was necessary to fabricate specimens with dimensions in accordance with ASTM standards. This was done by compression molding pellets of the specimens in a hot press at $200°C$. They are kept at

this temperature for 10-15 minutes to allow the particles fuse into one solid piece and then cooled.

Each sample was first molded in a rectangular plate mold with a cavity of dimensions $55 \times 55 \times 3mm$ (Figure 2a). A vacuum was applied to the mold while in the hot press (Figure 3), to eliminate porosity in the material. This process was repeated until a reasonable sample visibly free of voids was obtained. The resulting plate was then broken into small pieces which were again compression molded under the same conditions as above in a specimen mold (Figure 2b), to achieve its final dimensions. Figure 2b shows the specimen mold for a specimen used for fracture toughness tests.

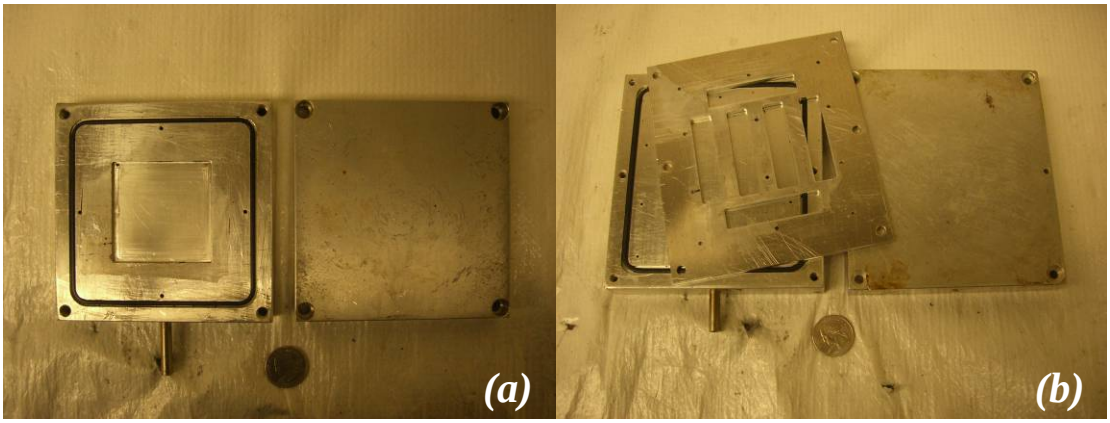

Figure 2 (a) Plate mold (b) Specimen mold for fracture toughness specimens.

The specimen fabrication process was repeated for the five different samples (neat, 0.1, 0.2, 0.3, and 1 wt% PS-SWCNT). A set of samples of neat and 1wt% PS-SWNT samples are shown in Figure 4.

Figure 3 Compression molding in a hot press with a vacuum applied to the mold.

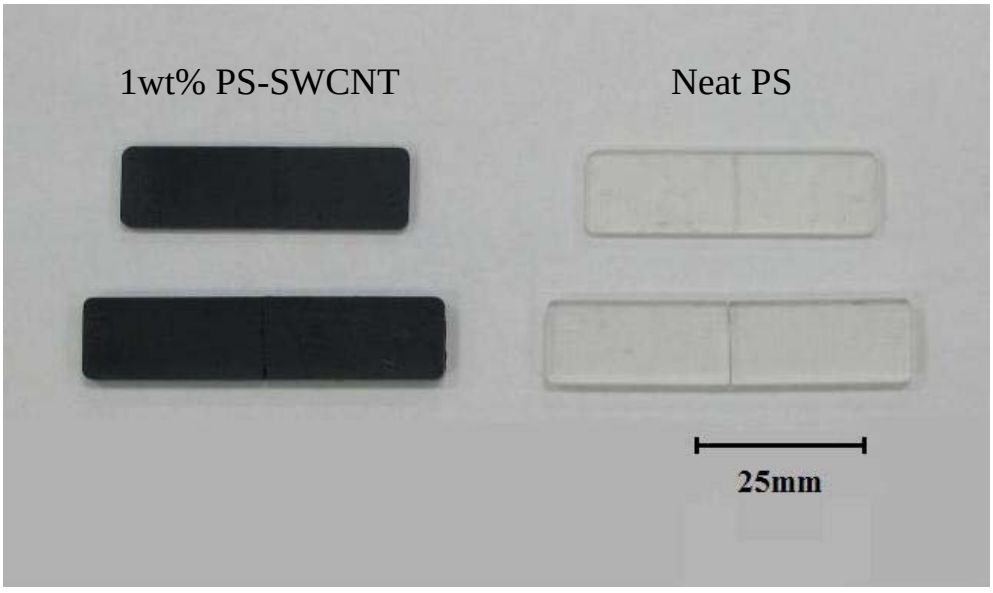

Figure 4 Flexural (top) and fracture toughness (bottom) specimens after compression molding in a hot press.

CHAPTER IV

EXPERIMENTAL

Three major tests were performed to characterize the PS-SWCNT material; flexural tests in 3 point bending to determine the elastic modulus and strength; fracture toughness tests to determine the fracture toughness in terms of the critical-stress-intensity factor, K_{Ic} and electrical tests to measure conductivity. Morphological studies were also carried out using SEM, and OM. This section discusses each test and some of the theory and considerations behind it.

4.1 Electrical Tests

Electrical tests were performed to determine the electrical conductivity of each sample. The sample dimensions for electrical testing were $12.7 \times 12.7 \times 2mm$. These tests were conducted in a QuadTech 7600 precision LCR meter. Silver paint on both sides of each specimen served as electrodes. Figure 5 is a schematic of the electrical tests. After connecting the sample to the LCR the conductivity is determined for frequencies ranging from 10 – 1000000Hz. The data is read into the computer using a LabVIEW interface.

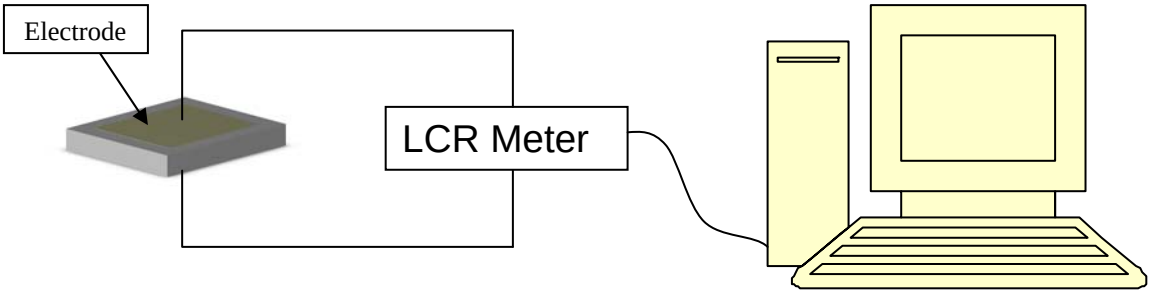

Figure 5 Schematic of instruments for making electrical measurements.

4.2 Flexural Testing

Flexural tests are used to determine the elastic modulus and flexural strength of a material in bending. It is particularly applicable to testing plastic materials since their applications often have them loaded in bending. Requirements for the design of the loading stage are outlined in the ASTM standards. The tests in this study were conducted in accordance to ASTM D790[17] to obtain the flexural modulus, strength and strain at failure of the materials. The specified geometry for the loading noses and supports of the loading stage are designed to minimize specimen indentation and the geometry of the sample is designed to ensure that specimen failure is by pure bending. Appendix A describes the design of the load stage used for flexural tests in 3 point bending.

The specimen dimensions used were $44.8 \times 12.7 \times 2mm$ requiring a load span of $32mm$. Five specimens of each sample were tested and their results averaged to obtain the reported values. Figure 6 shows a diagram of the test setup for a 3 point bend test and a moment diagram showing the moment distribution across the span of the specimen. From this diagram we observe that the 3 point bend test is designed to induce specimen

failure at the center of the specimen since this is the location of maximum stress. Also the stress distribution across the specimen thickness is such that the top is in compression and the bottom in tension. In brittle materials like PS failure generally occurs at the location of maximum tension.

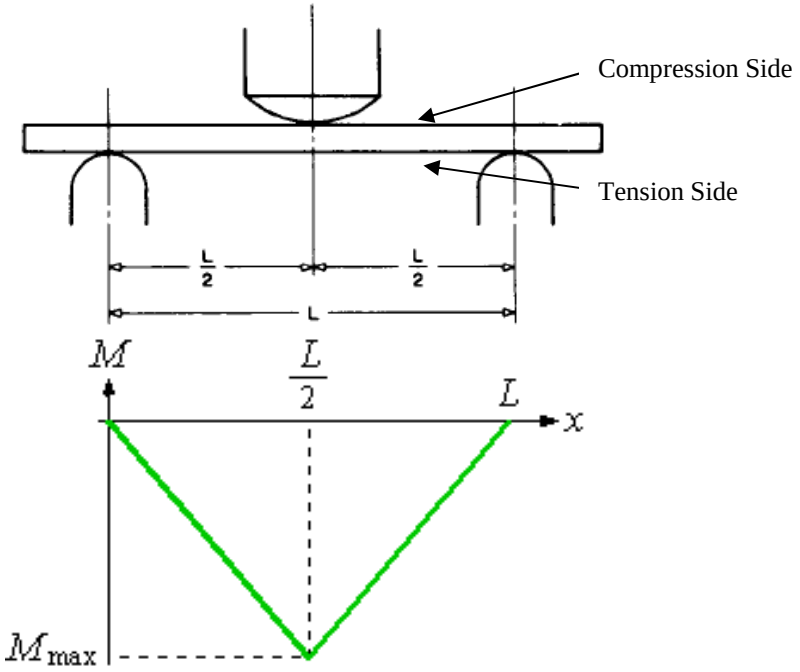

Figure 6 Schematic of a 3 point flexural test showing the variation of moment along the load span.

The specimen is strained at a rate of 0.01mm/mm/min as specified in the standards and the displacement D at the center of the beam, along with the load P applied on the specimen are recorded using an extensometer and a load cell. These are

used to calculate the stress (σ) and strain (ε) on the outer surface of the specimen at mid span using Equations (1) and (2).

$$\sigma = \frac{3PL}{2bd^2} \tag{1}$$

$$\varepsilon = \frac{6Dd}{L^2} \tag{2}$$

In the above equations P is the load applied, D is the mid-span displacement, L is the support span, b is the width of the specimen and d is the specimen thickness. Strength is determined by substituting P_{max} into P in equation (1) and the elastic modulus is determined as the initial slope of the stress strain curve after the initial settling region[17]. The strength of a material in a flexural test is very sensitive to the surface finish and quality, of the specimen since the surface experiences the highest tensile stress and is likely to be the site of failure initiation. Any voids or cracks on the surface are likely to act as stress concentrators and induce premature specimen failure so it is important that the surface be as smooth as possible.

4.3 Fracture Toughness Testing

Plain-strain fracture toughness tests were performed in accordance with ASTM D5045[18] to determine fracture toughness in terms of the critical stress intensity factor, K_{Ic} of the material. The single edge notch bend (SENB) specimen was used. Specimen dimensions were $55.8 \times 12.7 \times 3.175mm$ with a load span of $50.8mm$. The specimens were prepared by compression molding and a notch was cut into the specimen using a

jeweler's saw. A sharp crack was introduced by placing a fresh razor into the notch and gently tapping till a crack propagated ahead of the razor to about halfway across the specimen[18] (Figure 7).

Figure 7 SENB specimen showing a sharp natural crack.

After preparation the specimens were tested in bending at a crosshead rate of 10mm/min until failure. The maximum load was used to determine the K_{Ic} according to ASTM Standards.

CHAPTER V

RESULTS AND DISCUSSION

5.1 Electrical Properties

Figure 8 shows a graph of conductivity vs frequency for neat, 0.1, 0.2, 0.3 and 1wt% samples. For non-conductive materials conductivity shows a strong dependence on frequency which is the typical behavior of a capacitor[12]. This occurs for the neat material and materials with SWCNT concentrations below percolation. As the SWCNT loading increases the material becomes more conductive and looses this frequency dependence. These results indicate that the PS-SWCNT system becomes conductive between 0.1 and 0.2wt% SWCNT loading which compares well with some literature values[19,20]. Values ranging from 0.04wt%[21] to 11wt%[22] have been reported in the literature. The results are on the lower end of the range which indicates that a good dispersion of the SWCNT was achieved using the surfactant functionalization method.

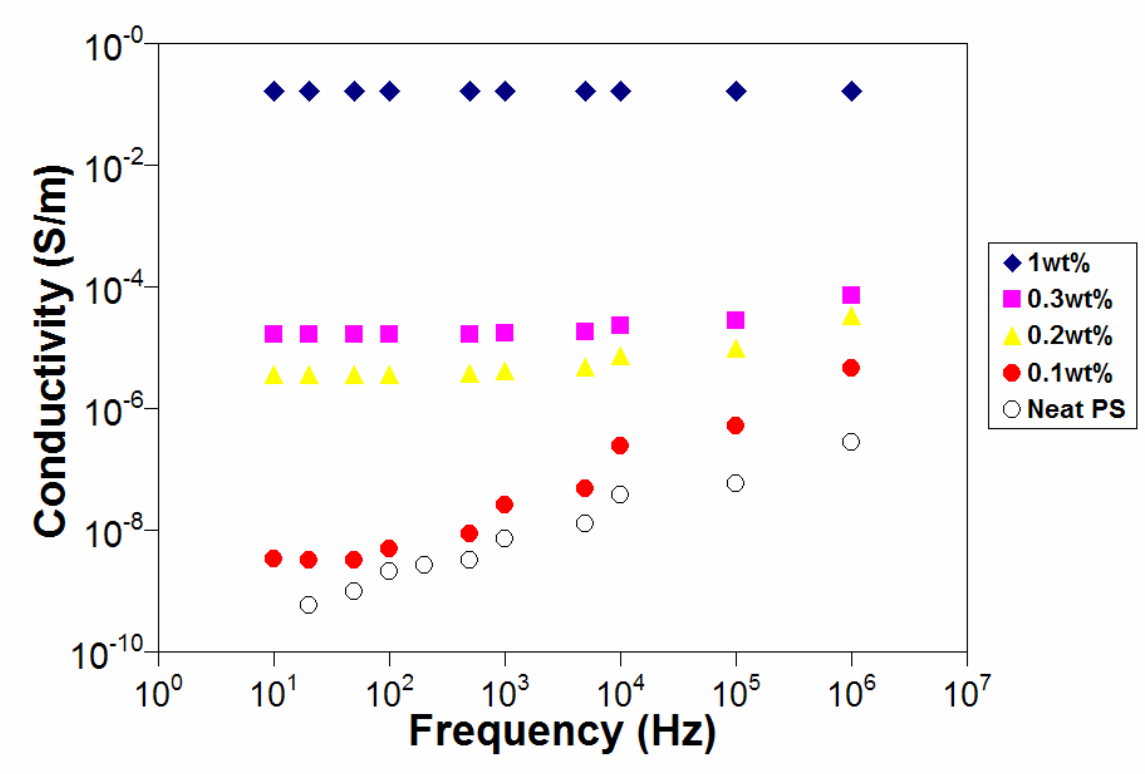

Figure 8 Conductivity vs. frequency graph showing frequency dependence in non-conductive materials while conductive materials are independent of frequency. Electrical percolation occurs between 0.1 and 0.2wt% .

A similar PS-SWCNT system was fabricated and characterized (Figure 9) by Zyvex[16], a nanotechnology company, using their own proprietary methods of dispersion. The resulting system shows a percolation threshold of only 0.045wt% which is one of the lowest reported in literature. Figure 9b compares the system in this study with the Zyvex system and shows some correlation at 1wt%. It is interesting to note that the Zyvex samples are very thin films 2-10 μm thick and as a result would tend to form a 2D network with the nanotubes aligned in the plane, to achieve percolation. The system in his study uses bulk samples and as a result may be expected to require higher

concentrations of nanotubes to achieve a 3D network. Approaching 1wt% there appears to be a convergence in the conductivity values of the 2D and 3D system.

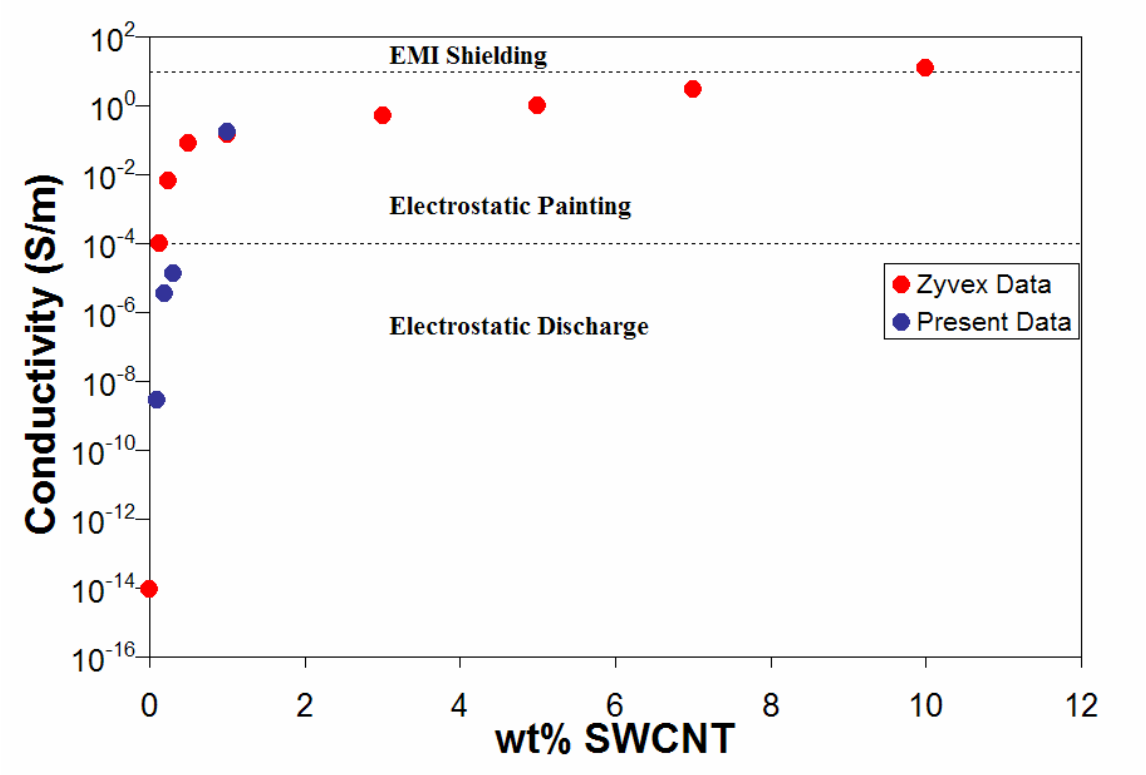

Figure 9 DC electrical conductivity vs SWCNT loading – A comparison of present results with results from Zyvex coorporation[16].

5.2 Flexural Properties

The PS-SWCNT material shows reasonably low electrical percolation values indicating that it may be useful as a multifunctional material with enhanced electrical properties, with the addition of just a small amount of SWCNT. To be truly

multifunctional though, it would be desirable that it at least maintain its mechanical properties. Flexural tests were carried out in 3pt bending according to ASTM D790 to determine the flexural strength and modulus of the material. This section discusses the results for these mechanical tests.

5.2.1 Neat Polystyrene

Figure 10 is a stress strain curve of a 3 point flexural test performed on neat PS. The material has a typical stress strain curve starting with a linear elastic region followed by a region of permanent deformation. Of particular interest in polystyrene is the nature of this permanent deformation or yielding. As reviewed earlier, the predominant yielding mechanism in PS and other glassy polymers is crazing. The craze initiation stress in the neat PS samples was estimated by a slope analysis of their stress-strain curves to be about 40MPa as shown in Figure 10. The nonlinear portion of the curve that follows is characterized by the initiation and stable growth of numerous crazes on the tension side of the specimen. Figure 11 is a vertical cross section of a specimen thickness showing these crazes. The fractured end is to the right of the image and the sample is oriented as it would be in a flexural test, with the tensile face to the bottom of the image and the compressive face to the top.

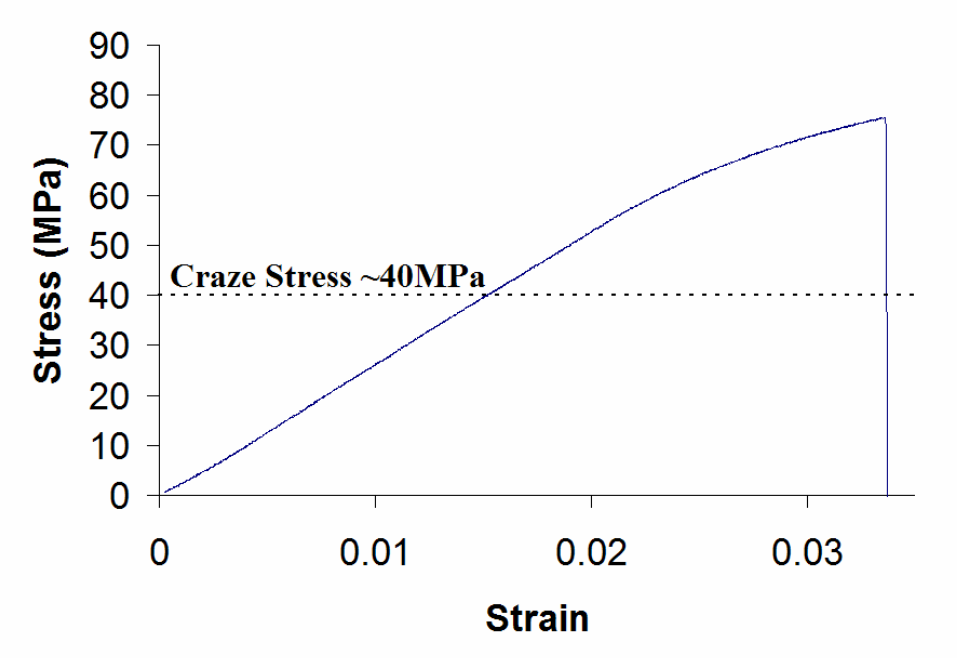

Figure 10 Stress strain curve of neat PS.

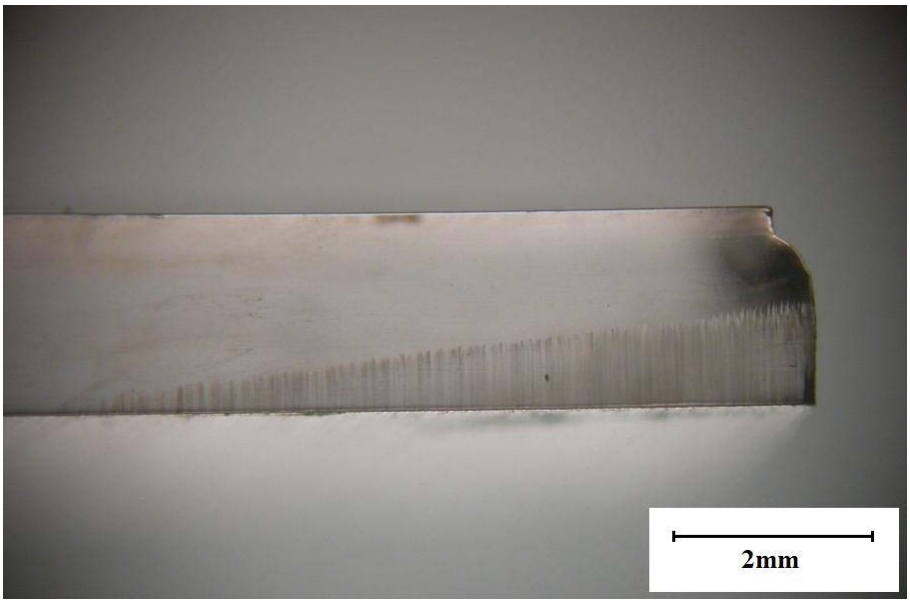

Figure 11 Side view of neat PS flexural specimen showing a wedge like feature caused by the formation of crazes of decreasing height with distance from the fracture surface (the point of maximum stress).

The crazes form a wedge-like feature starting at the fracture surface and decreasing in depth along the specimen length. The linear variation in depth corresponds to the linear stress distribution along the span of a simply supported beam and indicates that the depth of the craze at any location along the span corresponds to the stress at that location. The linear variation in the wedge provides proof that after initiation at a critical stress the craze depth grows in a stable manner with increasing stress on the specimen while new crazes initiate as neighboring surfaces reach the craze stress. Based on this insight one would expect that the stress at the tip of the wedge is close to the craze stress right before specimen failure. This stress may be calculated by measuring the location of the wedge tip along the specimen length, and calculating the stress at that location using a simple beam bending formula for a simply supported beam.

$$\sigma = \frac{My}{I} = \frac{3P_{\max}x}{bd^2} = 41.9MPa \tag{3}$$

where $M = \frac{P_{\max}}{2}x$, $y = \frac{d}{2}$ and $I = \frac{bd^3}{12}$

The result is close to the previously determined craze stress (~40MPa) which shows that stress conditions were favorable for the initiation of a craze at the wedge tip just before specimen failure. Specimen failure is by the breakdown of the first craze band (directly under the loading nose), after reaching about half way through the

specimen thickness. Figure 12 shows the fracture surface of a sample of neat PS. A smooth continuous surface is observed on the tension half or the specimen (lower half). This is a region of crazing. The region transitions to a rougher region on the compression side of the specimen. Figure 13 is an SEM image of the craze region revealing the presence craze fibrils characteristic of a craze.

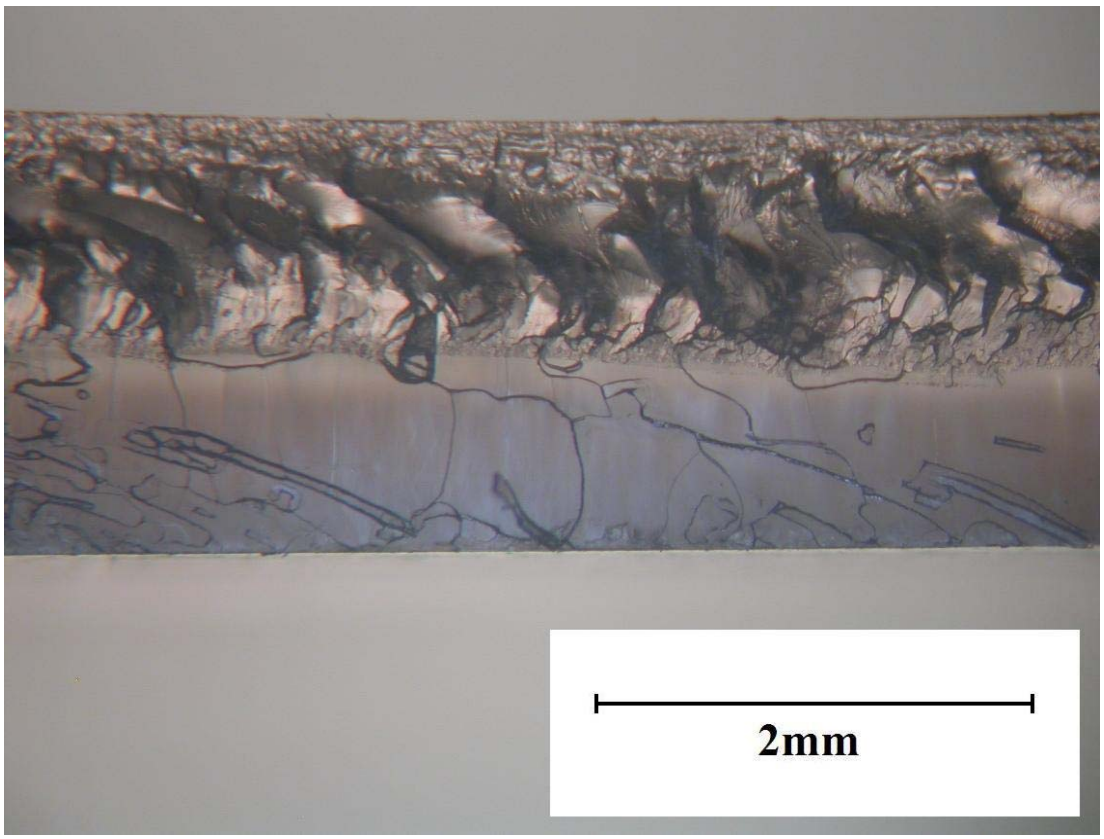

Figure 12 Fracture surface of neat PS showing the failed craze surface spanning half the specimen thickness.

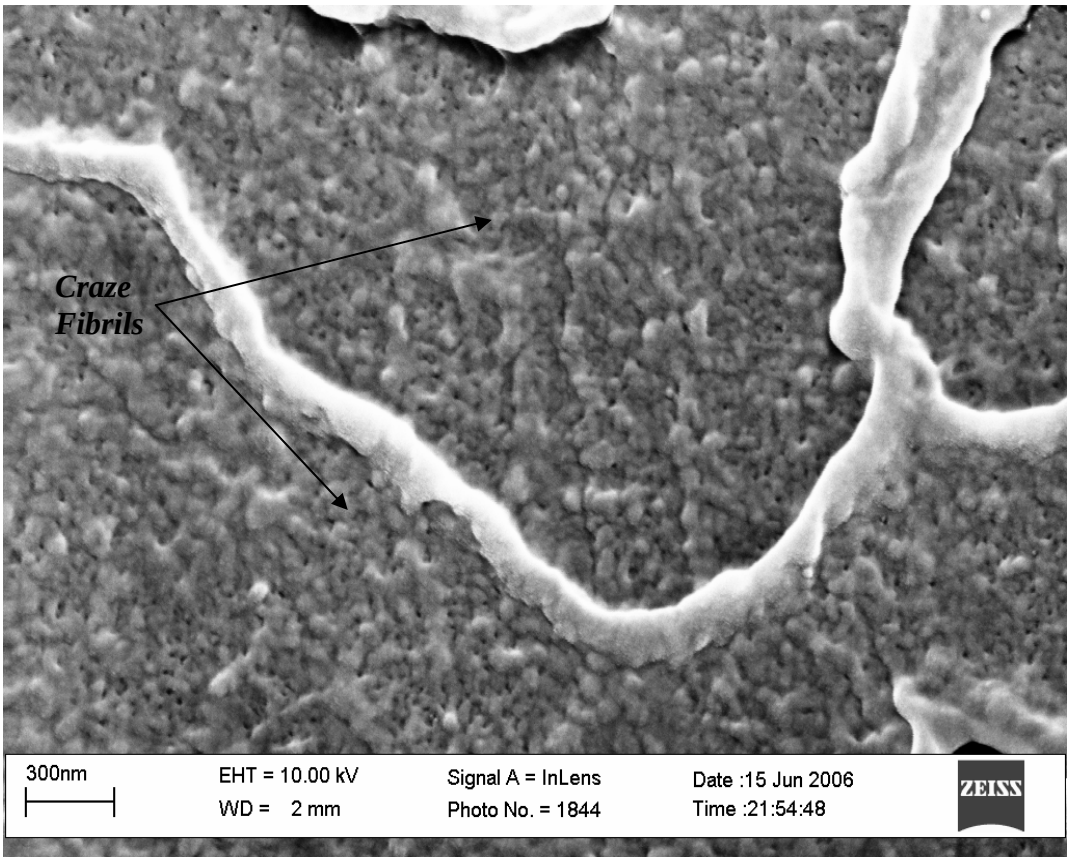

Figure 13 SEM image of the failed craze surface showing craze fibrils.

5.2.2 Polystyrene Nanocomposites

The nanocomposites were tested in a similar manner to the neat material. Figure 14 shows results from these tests compared to the neat material. There appears to be a minor increase in the stiffness of the nanocomposites but the values are not statistically significant. There is also an observed decrease in strength relative to the neat material. The following sections discuss these results.

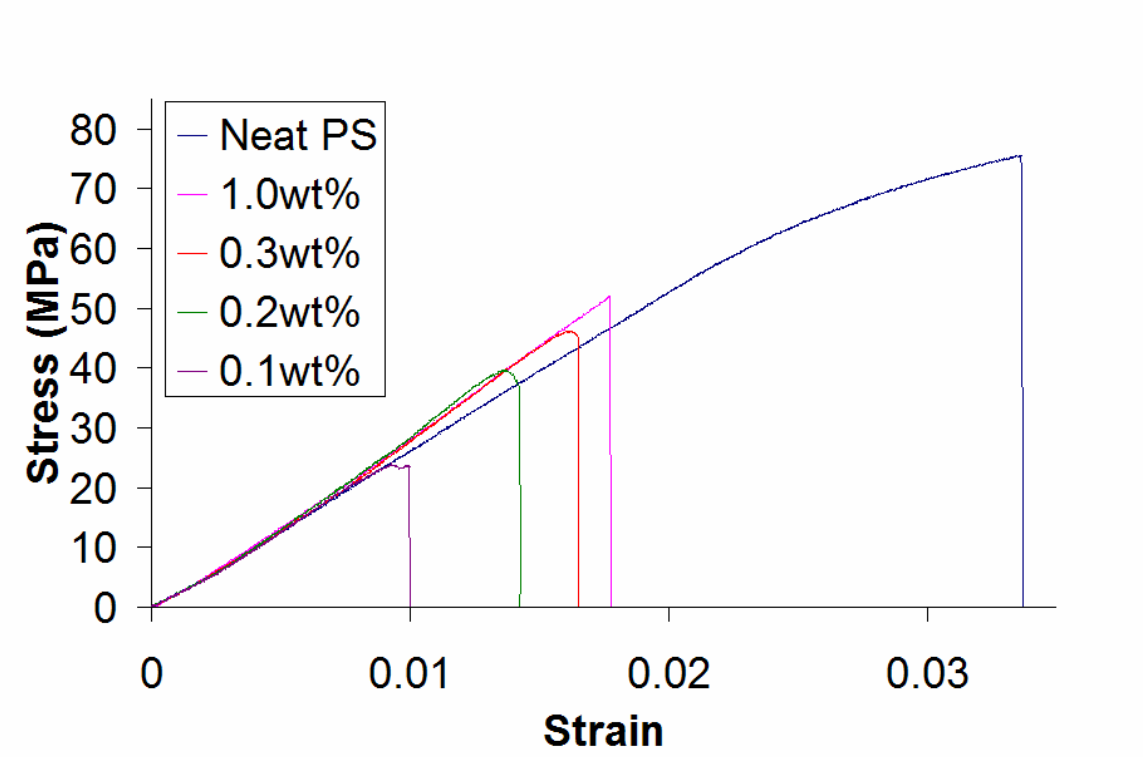

Figure 14 Flexural stress-strain curve showing changes in strength and yielding behavior for different PS-SWNT nanocomposites.

5.2.2.1 Flexural Strength

Table I summarizes the results for the flexural strength and strain in the neat and nanocomposite materials. Figure 14 presents the stress strain curves and Figure 15 is a graphical representation of the strength at different SWCNT loadings. The flexural strength of the PS-SWCNT material decreases dramatically in the 0.1wt% material

compared to the neat material. This is followed by a gradual increase to 0.2, 0.3, and 1wt%.

The sudden decrease in the strength of the nanocomposite at 0.1wt% compared to the neat material indicates that at this level the nanotubes are acting more like stress concentrators than reinforcing particles. It is interesting to note that this stress concentration appears to be about two, relative to the craze stress of the neat material i.e. the nanocomposite at 0.1 wt% fails at $\sim 1/2$ the craze stress. This is similar to the stress concentration of a spherical particle in a 3D matrix[23].

TABLE I
Test Results for Flexural Strength and Strain at Failure

SWNT Loading (wt%)	Flexural Strength (MPa)	Strain at Failure
0.0	76.3 ± 1.1%	3.3% ± 1.7%
0.1	23.4 ± 9.3%	0.9% ± 6.1%
0.2	37.1 ± 9.6%	1.2% ± 7.5%
0.3	41.3 ± 9.4%	1.6% ± 8.3%
1.0	48.8 ± 7.4%	1.7% ± 4.2%

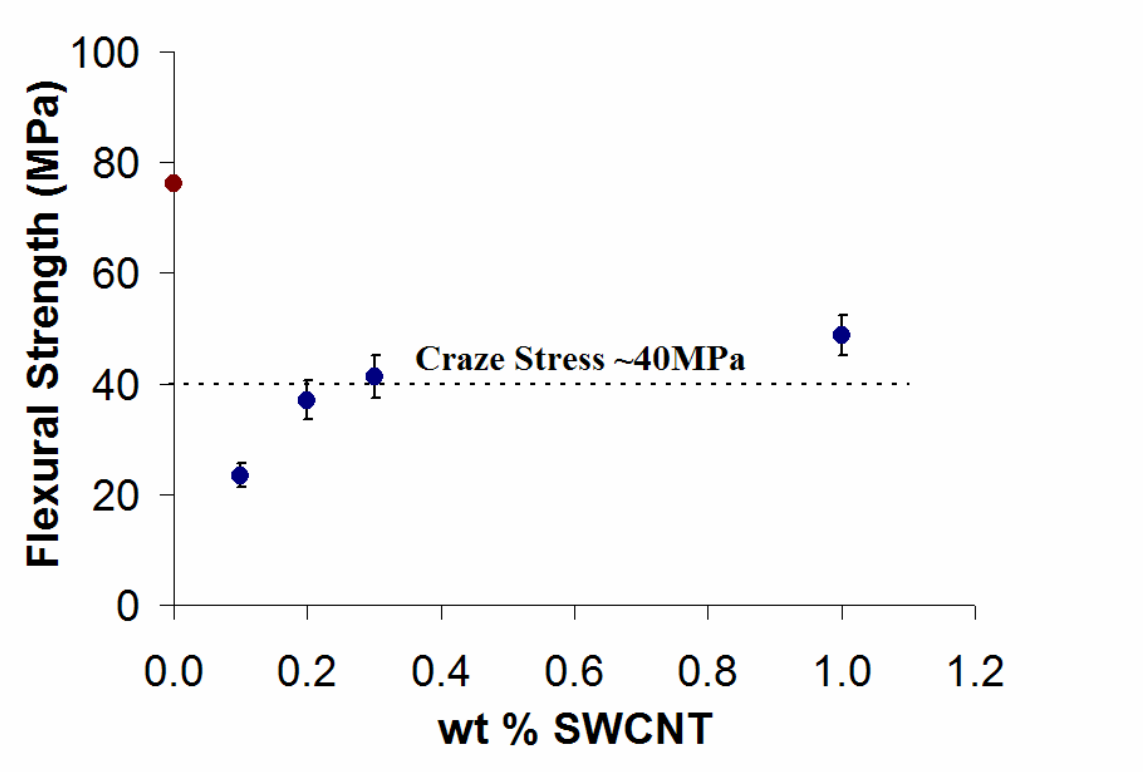

Figure 15 Comparison of the trend in flexural strength of PS-SWNT at different wt%, with the craze stress of the neat material.

The behavior of increasing strength with increasing nanotube loading from 0.1 – 1wt% is rather unusual from a stress concentration point of view because one would expect a higher number of stress concentrators to cause a decrease in strength. This has been observed in previous work on PS containing glass beads[24]. Instead we observe a gradual increase in strength with the 1wt% material failing at a stress significantly above the neat material craze stress. The observed increase in strength with nanotube content is likely due to a mechanism the effect of which gets stronger with increasing nanotube content. One such mechanism is the formation of networks by the nanotubes. Evidence

of network formation is present in the results of electrical tests performed on nanocomposite systems since these networks are responsible for making the material conductive by forming a continuous path for electron flow. The formation of networks may play a part in the strength increase observed in the nanocomposites. Networks of nanotubes in the PS matrix would have the ability to hold it together and the potential to form their own entanglements similar to polymer entanglements which keep the polymer together and gives it strength.

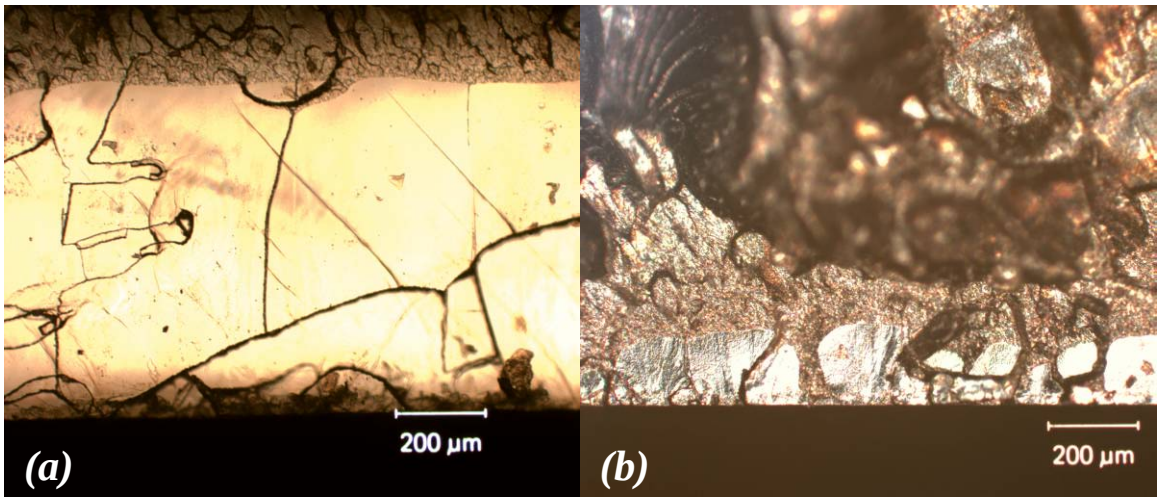

Figure 16 Optical micrographs comparing fracture surfaces of neat PS and 1wt% PS-SWNT. (a) Neat PS:The craze band spans the specimen width and the half of its depth in tension (b) 1wt% PS-SWNT: There is a thin craze band spanning the width of the specimen at the edge where the tensile force is maximum.

Optical micrographs of the fracture surface of the 1wt% material (Figure 16b) show craze surface similar to the one observed in neat PS (Figure 16a). The surface spans the entire width of the specimen close to the max tension surface indicating that it is not due to a specific surface flaw. SEM micrographs show similarities in the craze morphology of neat and 1wt% materials (compare Figure 17 to 18 and Figure 19 to 20). The evidence indicates a similar progression of events to that previously outlined for the neat material except that after initiation, the craze growth is not sustained. Rather the craze breaks down resulting in an early transition to rapid crack growth causing brittle failure. This early transition indicates that the craze is unable to grow in a stable manner, as in the neat material, in the presence of nanotubes. The result is that the 1wt% material fails with little craze yielding. The difference between the neat and 1wt% material therefore appears to be their differing abilities to sustain stable craze growth. The decrease in strength therefore appears to be caused by a hindrance of the natural toughening mechanism of PS.

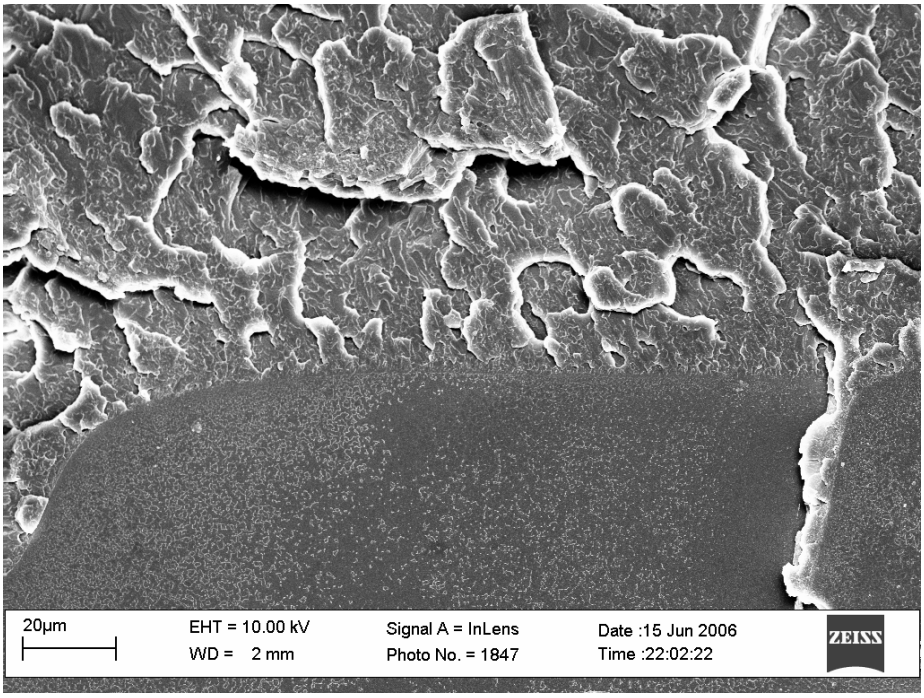

Figure 17 Transition from craze region to brittle fracture region in neat PS.

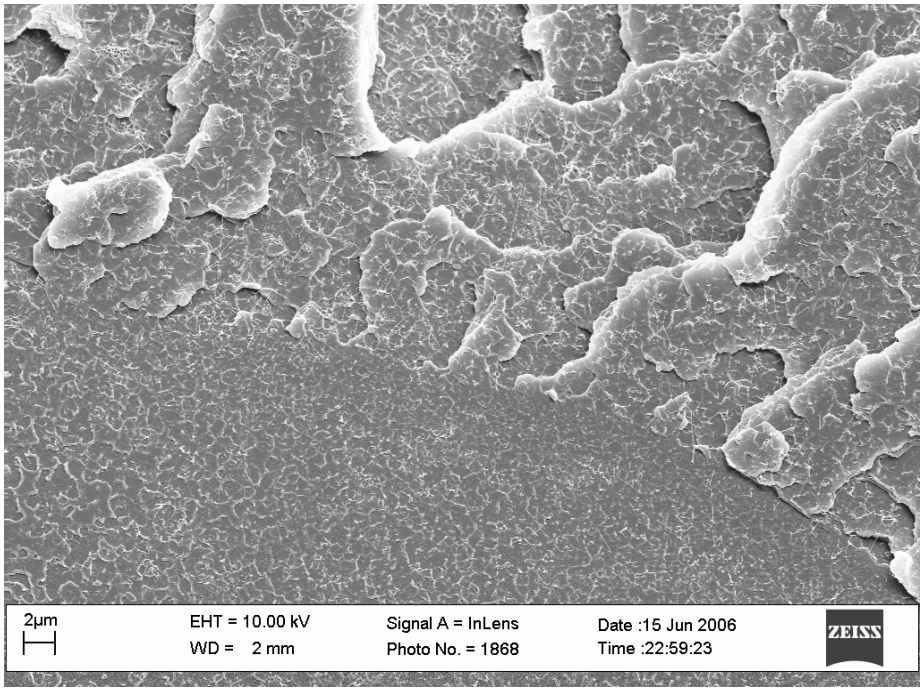

Figure 18 Transition from craze region to brittle fracture in 1wt% PS-SWNT.

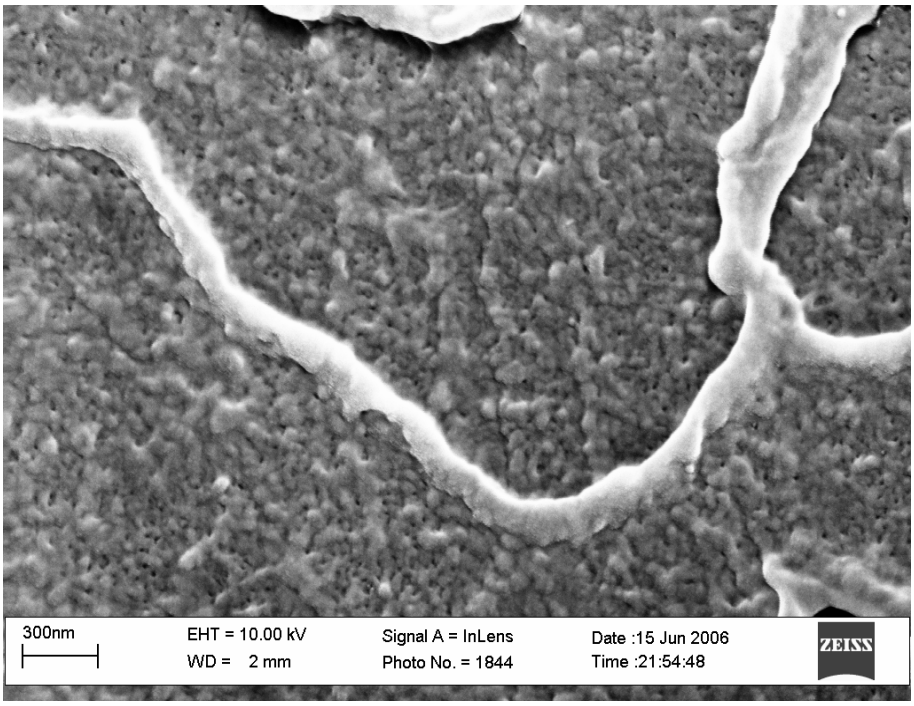

Figure 19 High magnification of the craze surface in neat PS.

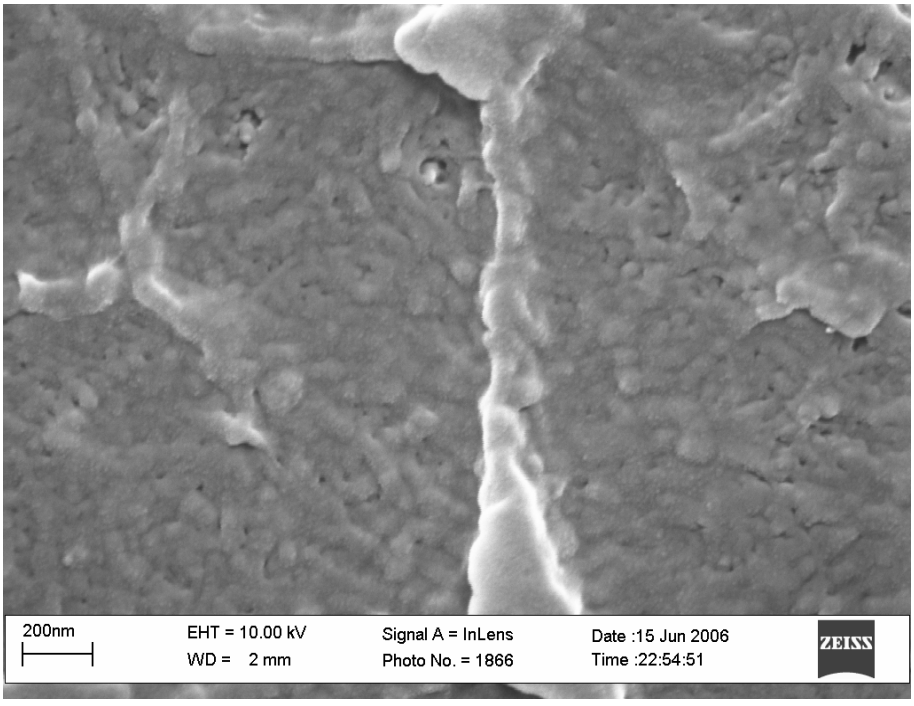

Figure 20 High magnification of the craze surface in 1wt% PS.

5.2.2.2 Flexural Modulus

TABLE II
Test Results for Flexural Modulus of PS-SWCNT

SWNT Loading (wt%)	Flexural Modulus (MPa)	Normalized Modulus
0.0	2731 ±1.2%	1.000
0.1	2851 ±2.1%	1.043
0.2	2857 ±2.8%	1.046
0.3	2711 ±2.7%	0.992
1.0	2881 ±2.7%	1.055

Table II is a summary of he results obtained from flexural testing of the PS-SWNT at different loadings of CNT. They show a minor increase in the flexural modulus of the material with increasing SWCNT loading. This increase is not significant since most of the values fall within the errors of others. The maximum improvement is in the 1wt% material; about 5% above the stiffness of the neat material. SEM results and the results of electrical characterization show that a good dispersion has been achieved and the system consists of randomly oriented nanotubes. Figure 21 shows loose nanotubes on the surface of the material. This suggests that they were easily pulled out of the matrix during fracture which is evidence of a weak interfacial interaction between the nanotubes and the matrix material and a possible explanation for the lack of improvements in the stiffness of the nanocomposite material.

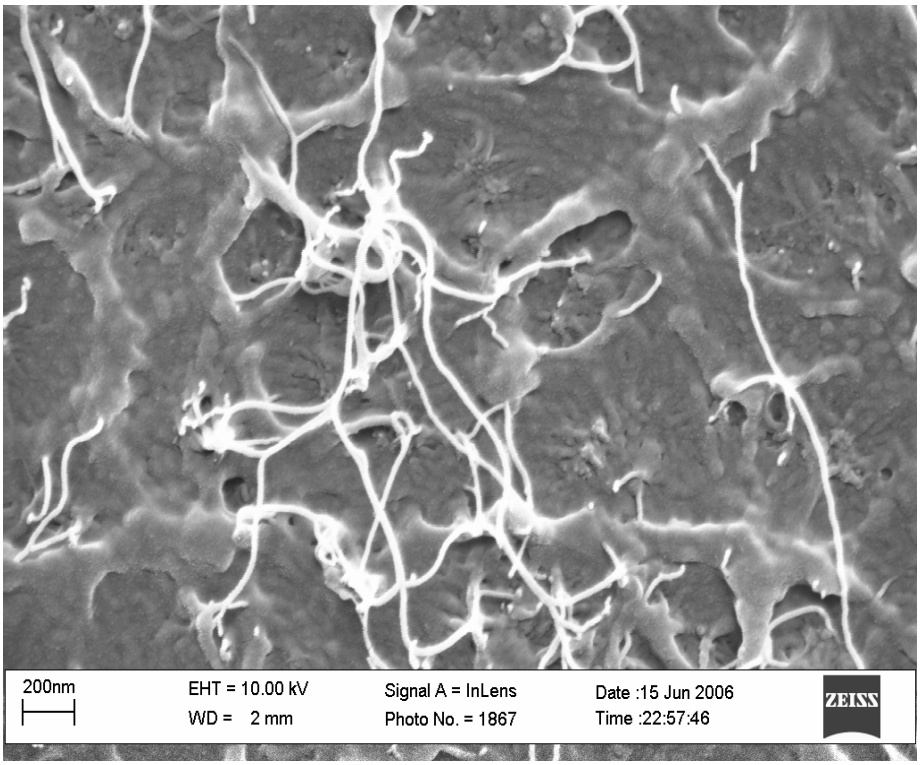

Figure 21 SEM image showing a weak of interaction between the nanotubes and the PS matrix.

5.3 Fracture Toughness Properties

Tests were performed to determine fracture toughness in terms of the critical-stress-intensity factor K_{Ic}. Figure 22 shows the trend of K_{Ic} with increasing SWCNT loading. The values are summarized in Table III. The results show a general decrease in the fracture toughness of the materials with increasing SWCNT loading. These results are in agreement with the observed decrease in the yielding of the nanocomposite materials with increase in SWCNT loading (Figure 14).

TABLE III
Test Results for K_{Ic} of PS and PS-SWCNT at Different SWCNT Loadings

SWCNT Loading (wt%)	K_{Ic} (MPa $m^{1/2}$)
0.0	1.98 ±7.6%
0.2	1.22 ±6.1%
0.3	1.35 ±6.9%
1.0	0.83 ±6.4%

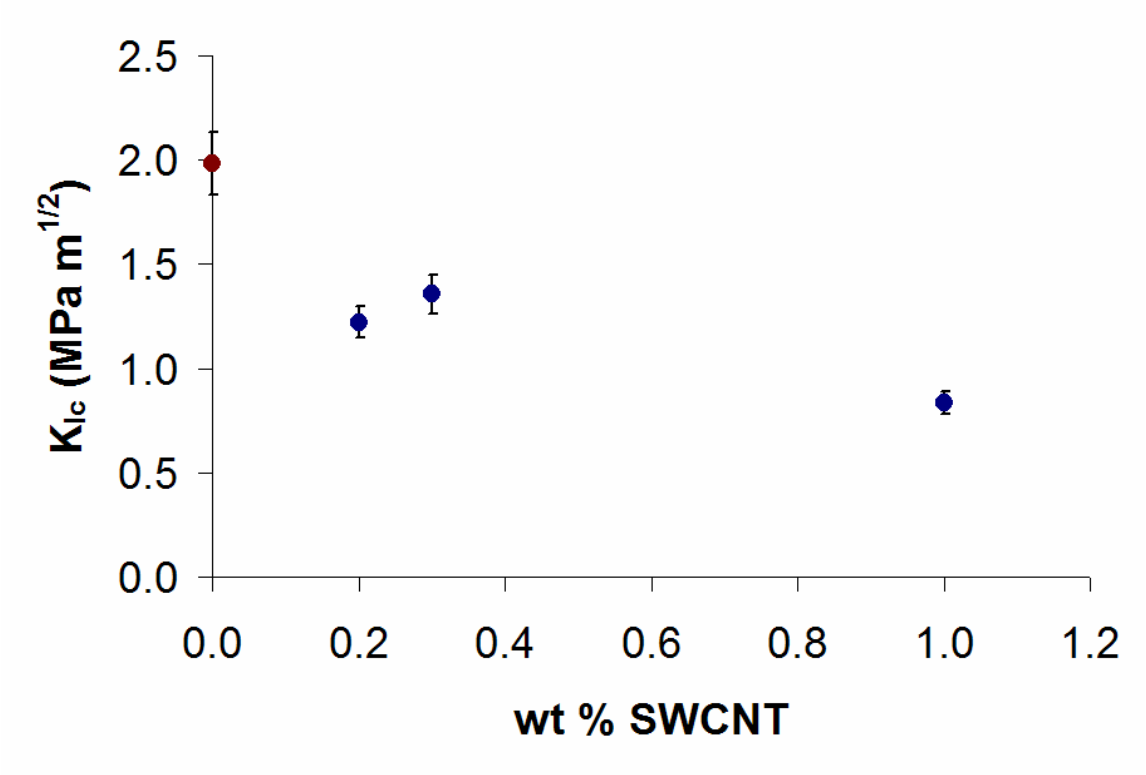

Figure 22 Fracture toughness (K_{Ic}) of neat PS and PS-SWNT nanocomposites.

During fracture testing crack propagation is often preceded by for formation of a damage zone at the crack tip. The mechanisms that create this damage zones are various toughening mechanisms such as shear banding and crazing. These damage mechanisms

require energy so the larger the damage zone, the more resistant the material is to the propagation of a sharp crack. SEM images of the fracture surface of the neat material show clear evidence of a damage zone before the crack propagation as indicated on Figure 23. The damage zone is not as easily observed in the nanocomposites (Figure 24 - 26), which explains their decrease in toughness relative to the neat material.

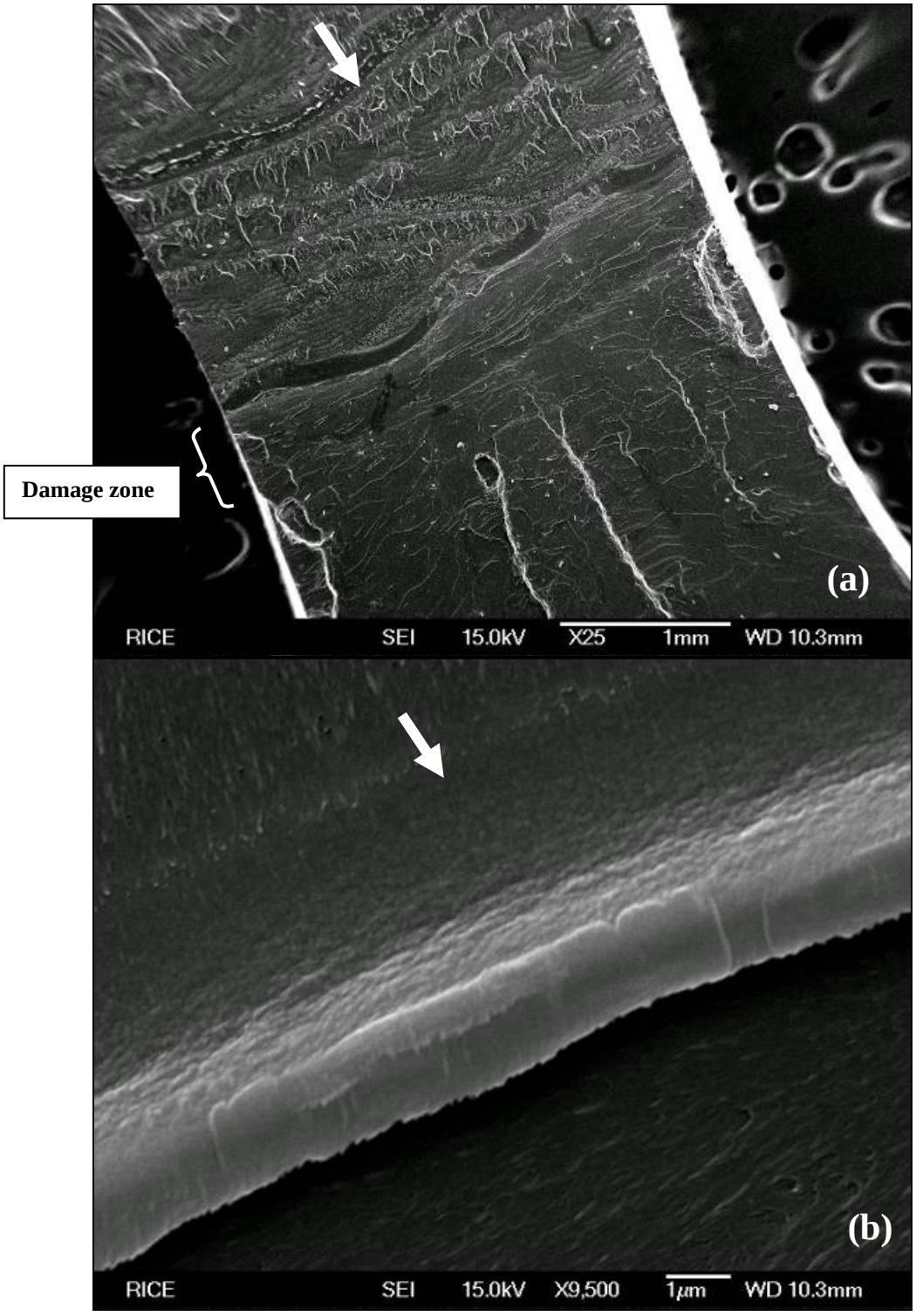

Figure 23 (a) SEM image of the fracture surface of a fracture toughness sample of neat PS showing a damage zone across the specimen thickness (b) higher magnification of the fracture surface. Arrows indicate the direction of crack propagation.

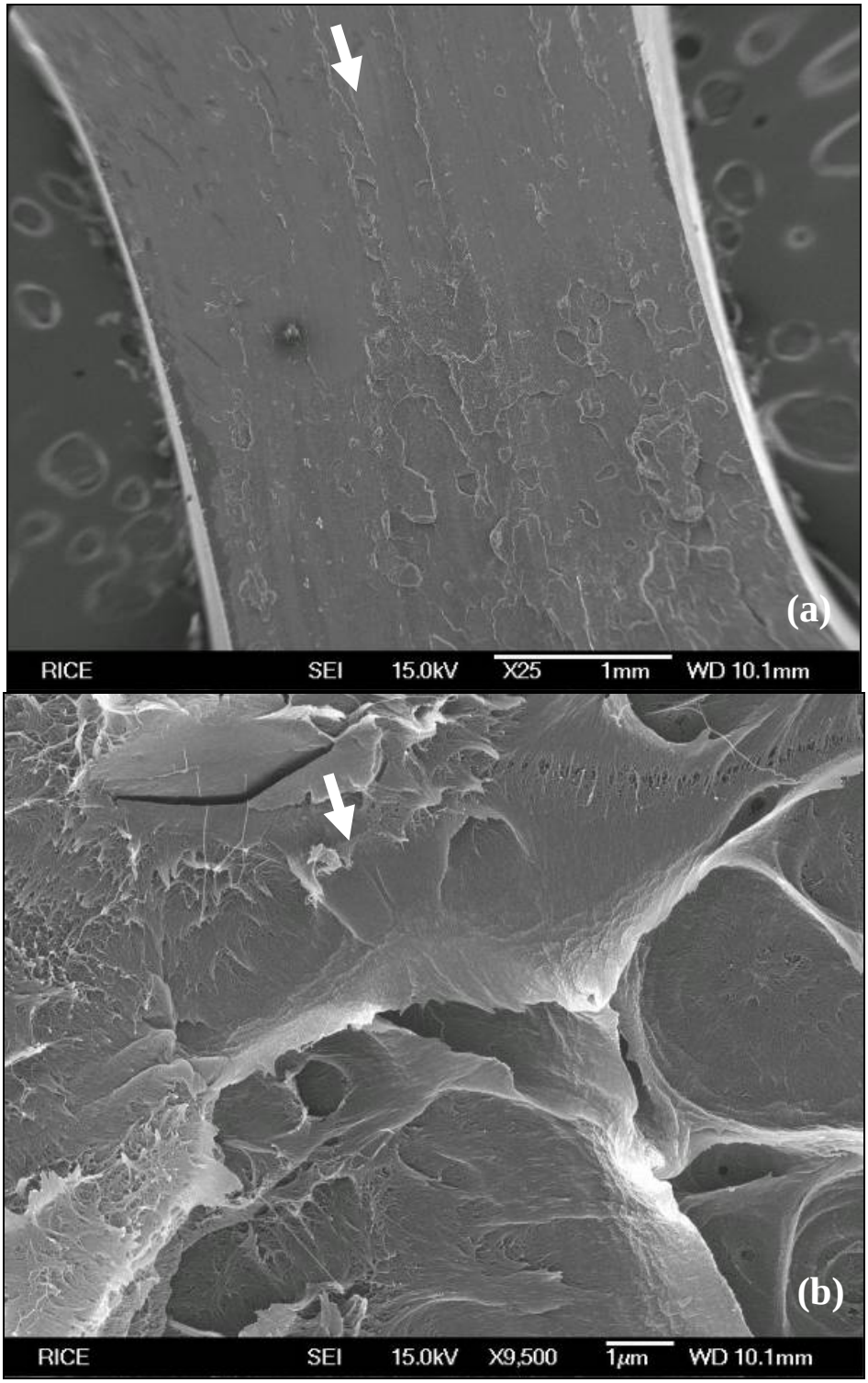

Figure 24 (a) SEM image of the fracture surface of a fracture toughness sample of 0.2wt% PS (b)higher magnification of the fracture surface. Arrows indicate the direction of crack propagation.

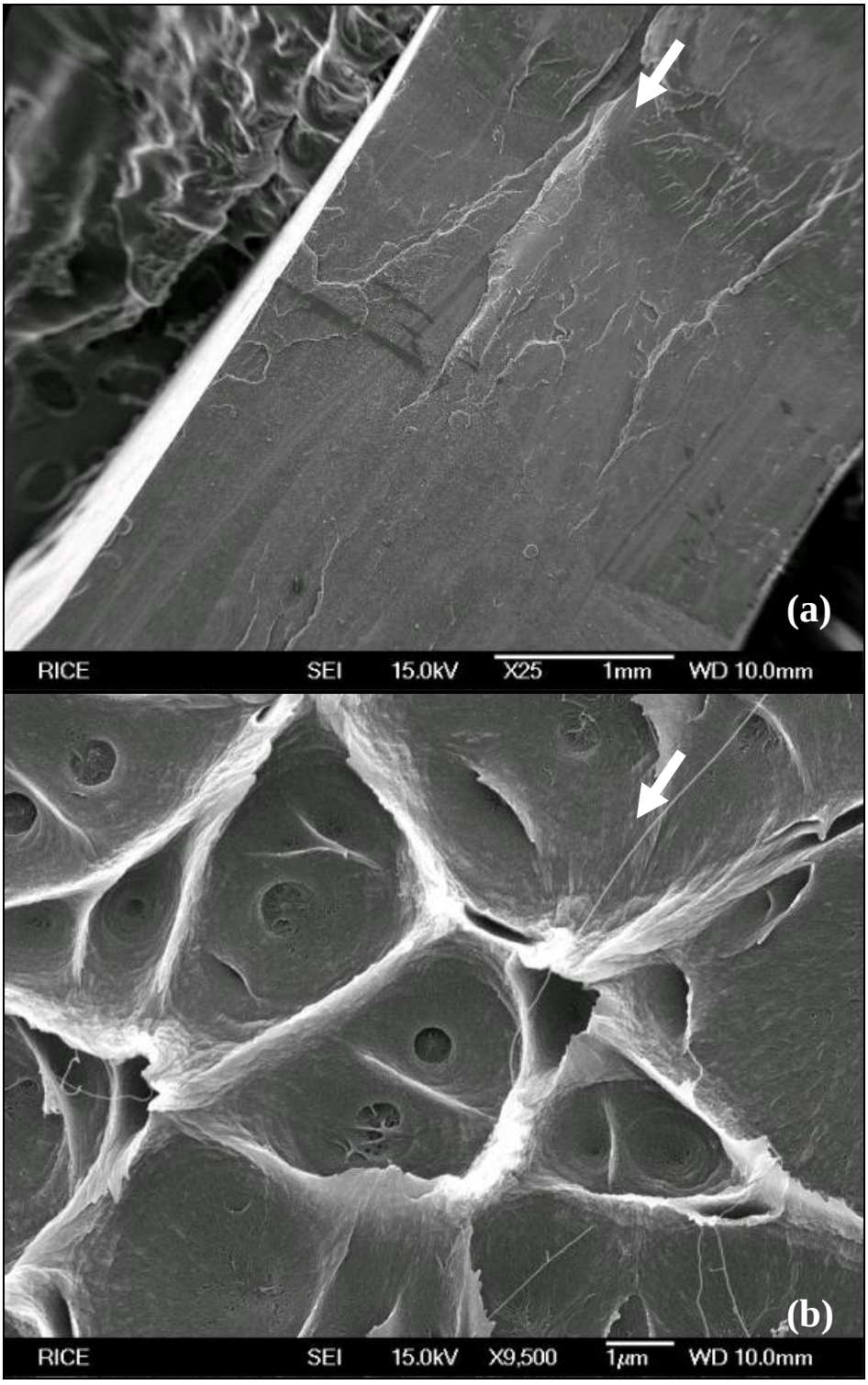

Figure 25 (a) SEM image of the fracture surface of a fracture toughness sample of 0.3wt% PS (b)higher magnification of the fracture surface. Arrows indicate the direction of crack propagation.

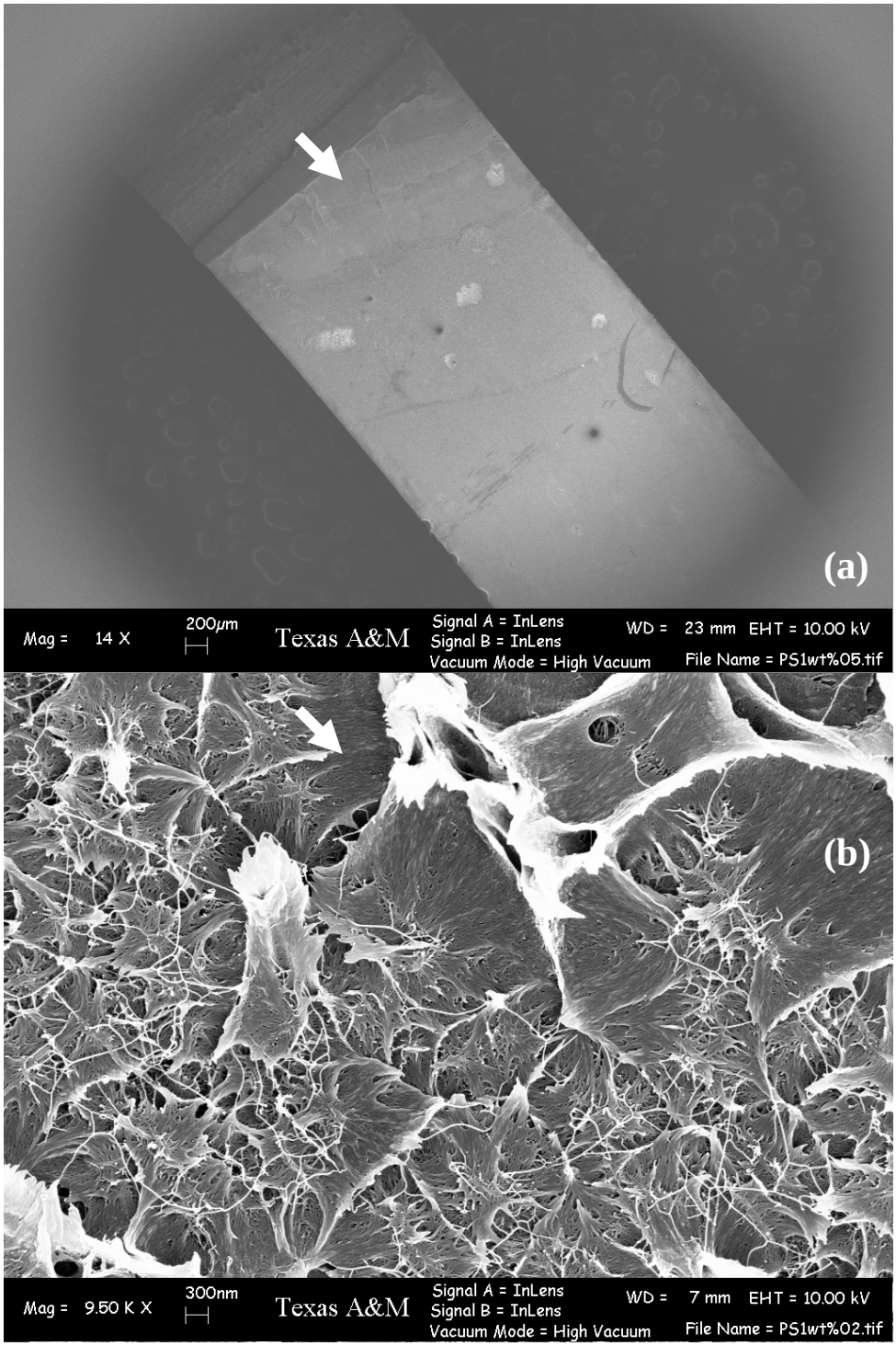

Figure 26 (a) SEM image of the fracture surface of a fracture toughness sample of 1wt% PS (b)higher magnification of the fracture surface. Arrows indicate the direction of crack propagation.

CHAPTER VI

CONCLUSION

We performed electrical and mechanical tests to characterize a nanocomposite of polystyrene containing SWCNT dispersed using a CTAB surfactant. The results show a five order of magnitude increase in conductivity at just 0.3 wt% SWCNT. The electrical percolation occurs between 0.1and 0.2 wt% (Figure 8) which is low compared to values in literature.

Mechanical test results show a decrease in strength of the nanocomposites relative to the neat material. A substantial drop in strength at 0.1wt% loading and a subsequent increase at 0.2, 0.3 and 1wt% was observed. The initial decrease in strength is attributed to a stress concentration phenomenon at the lower weight fractions of SWCNT. Evidence from micrographs (Figure 16) indicate that at 1wt% the material initially forms a craze but it quickly breaks down resulting in a more brittle behavior and a lower strength than the neat material. The neat material is able to form multiple stable crazes, resulting in extensive permanent deformation before final failure. The craze instability at 1wt% appears to be as a result of the presence of nanotubes.

The flexural modulus shows little increase with the addition of SWCNTs. This may result from a weak interaction of the nanotubes with the matrix, the evidence of which is observed in Figure 21.

The results of fracture toughness tests show a general decrease in the K_{Ic} of the nanocomposites with increasing nanotube content. Evidence of a damage zone is

observed in the neat material but not in the nanocomposites indicating that nanotubes in some way hinder crazing, the natural damage mechanism of PS.

Overall the results show a decrease in mechanical properties and point to one common cause. The nanotubes appear to hinder the ability of the material to sustain the growth of stable crazes and leads to reductions in the mechanical properties that depend on this mechanism.

REFERENCES

1. Thostenson, E. T.; Li, C.; Chou, T. W., Composites Science and Technology 2005, 65, 491.

2. Iijima, S., Nature 1991, 354, 56.

3. Schmitt, C.; Lebienvenu, M., Journal of Materials Processing Technology 2003, 134, 303.

4. Yurekli, K.; Mitchell, C. A.; Krishnamoorti, R., JACS 2004, 126, 9902.

5. Thostenson, E. T.; Ren, Z.; Chou, T. W., Composites Science and Technology 2001, 61, 1899.

6. Saito, R.; Fujita, M.; Dresselhaus, G.; Dresselhaus, M. S., Applied Physics Letters 1992, 60, 2204.

7. Bronikowski, M. J.; Willis, P. A.; Colbert, D. T.; Smith, K. A.; Smalley, R. E., J. Vac. Sci. Technol. 2001, 19, 1800.

8. Kramer, E. J., Advances In Polymer Science 1983, 52, 1.

9. Marshall, G. P.; Culver, L. E.; Williams, J. G., International Journal of Fracture 1973, 9, 295.

10. Maestrini, C.; Kramer, E. J., Polymer 1991, 32, 609.

11. Argon, A. S.; Cohen, R. E.; Gebizlioglu, O. S.; Schwier, C. E., Advances in Polymer Science 1983, 52-53, 275.

12. Ounaies, Z.; Park, C.; Wise, K. E.; Siochi, E. J.; Harrison, J. S., Composites Science and Technology 2003, 63, 1637.

13. Sheng, N.; Boyce, M. C.; Parks, D. M.; Rutledge, G. C.; Abes, J. I.; Cohen, R. E., Polymer 2004, 45, 487.

14. Thostenson, E. T.; Chou, T.-W., Journal of Physics D: Applied Physics 2002, 35, L77.

15. Qian, D.; Dickey, E. C.; Andrews, R.; Rantell, T., Applied Physics Letters 2000, 76, 10.

16. Rutkofsky, M.; Banash, M.; Rajagopal, R.; Chen, J. in Zyvex Application Note 9709; Zyvex Corporation: Dallas Texas: 2006.

17. Annual Book of ASTM Standards 2002, vol 08.01

18. ASTM D5045 Annual Book of ASTM Standards 1999, Vol 08.02

19. Benoit, J. M.; Corraze, B.; Lefrant, S.; Blau, W. J.; Bernier, P.; Chauvet, O., Synthetic Metals 2001, 121, 1215.

20. Biercuk, M. J.; Llaguno, M. C.; Radosavljevic, M.; Hyun, J. K.; Fischer, J. E.; Johnson, A. T., Applied Physics Letters 2002, 80, 2767.

21. Grunlan, J. C.; Mehrabi, A. R.; Bannon, M. V.; Bahr, J. L., Advanced Materials 2004, 16, 150.

22. Kymakis, E.; Alexandou, I.; Amaratunga, G. A. J., Synthetic Metals 2002, 127, 59.

23. Wang, Q. Z., The Journal of Strain Analysis for Engineering Design 2002, 37, 259.

24. Dekkers, M. E. J.; Heikens, D., Journal of Applied Polymer Science 1983, 28, 3809.

APPENDIX A

LOADING STAGE DESIGN AND FABRICATION

In order to conduct flexural tests it was necessary to design and fabricate a loading stage that would fit in an MTS frame. This is a brief description of the design and fabrication of the frame.

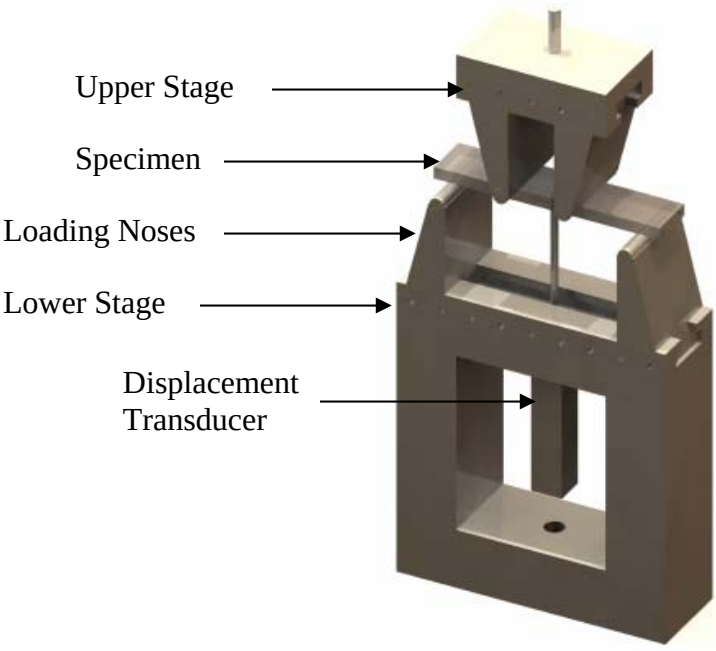

Figure 27 MTS Loading stage for flexural tests in 3pt and 4pt bending.

The loading stage was designed according to ASTM D790 and D6272 for flexural testing in 3pt and 4pt bending. These standards require specimens to have a span

to thickness ratio of 16:1 with enough additional length to provide enough hang-over to prevent slippage from the supports. The stage dimensions were determined based on a projected range of sample sizes that might be tested on the frame. It was designed to have variable span, loading and support noses, so that it would be robust enough to test different sample dimensions. The loading nose diameter was specified as 0.25in to minimize sample indentation during testing which might lead to errors in test data.

The Displacement transducer shown in Figure 27 is only necessary when testing in 4pt bending. The internal displacement transducer of the MTS can be used when testing in 3pt bending since the displacement at the center of the specimen span is identical to the MTS displacement. Following are plans for the individual components of the loading stage. All components are made of aluminum except the dowels which are made of steel.

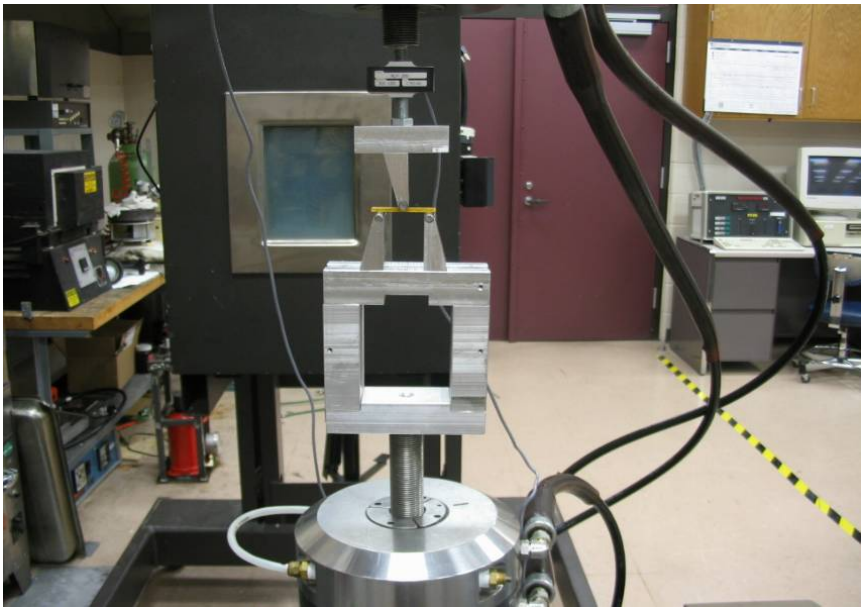

Figure 28 Loading stage in MTS machine.

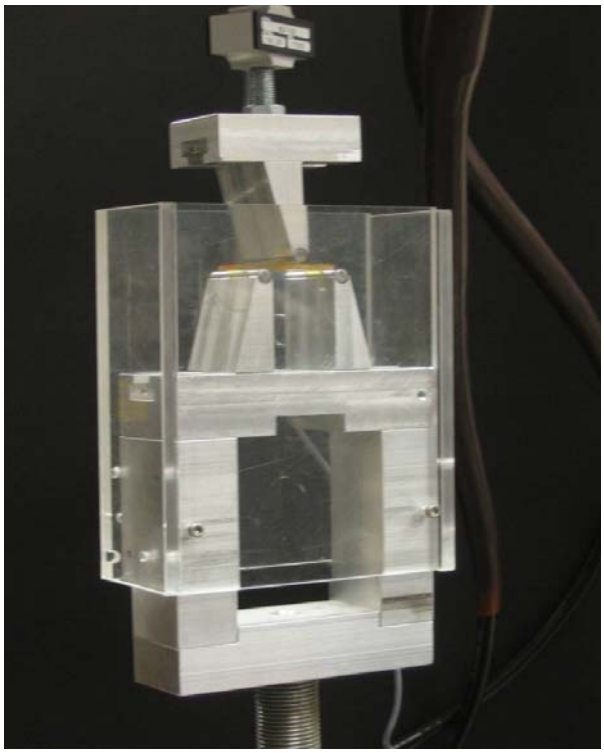

Figure 29 Loading stage in 3pt bending configuration with plexiglas shield.

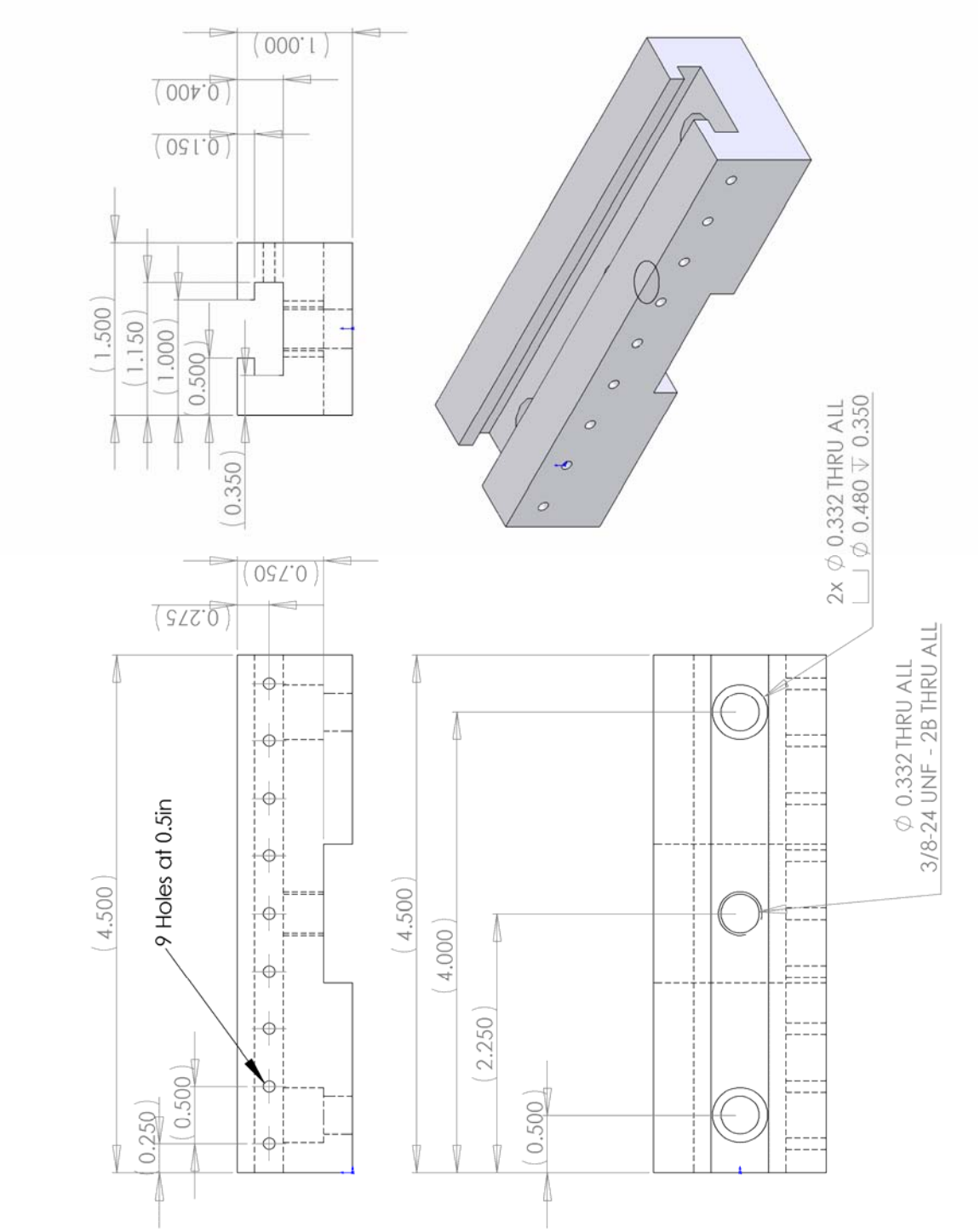
(1.000)
(0.400)
(0.150)
(1.500)
(1.150)
(1.000)
(0.500)
(0.350)
(0.750)
(0.275)
(4.500)
9 Holes at 0.5in
(0.250)
(0.500)
2x ⌀ 0.332 THRU ALL
⌴ ⌀ 0.480 ↧ 0.350
⌀ 0.332 THRU ALL
3/8-24 UNF - 2B THRU ALL
(4.500)
(4.000)
(2.250)
(0.500)

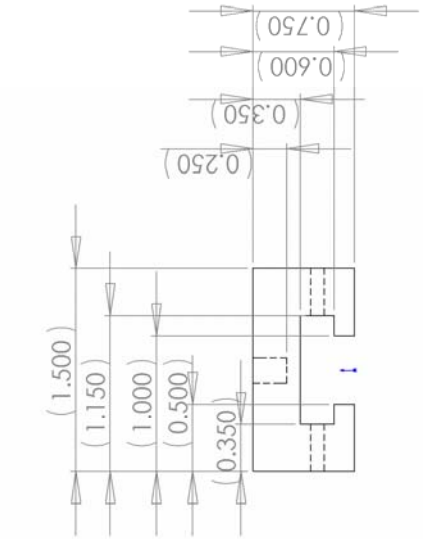
(0.750)
(0.600)
(0.350)
(0.250)
(1.500)
(1.150)
(1.000)
(0.500)
(0.350)

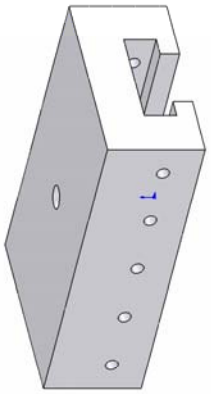

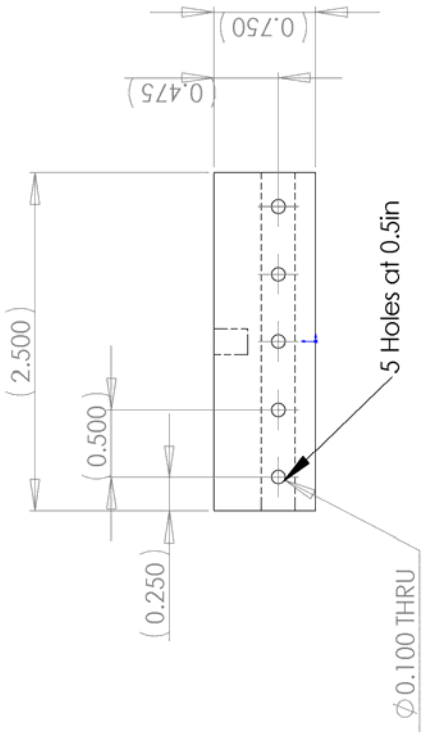
(0.750)
(0.475)
(2.500)
(0.500)
(0.250)
5 Holes at 0.5in
⌀0.100 THRU

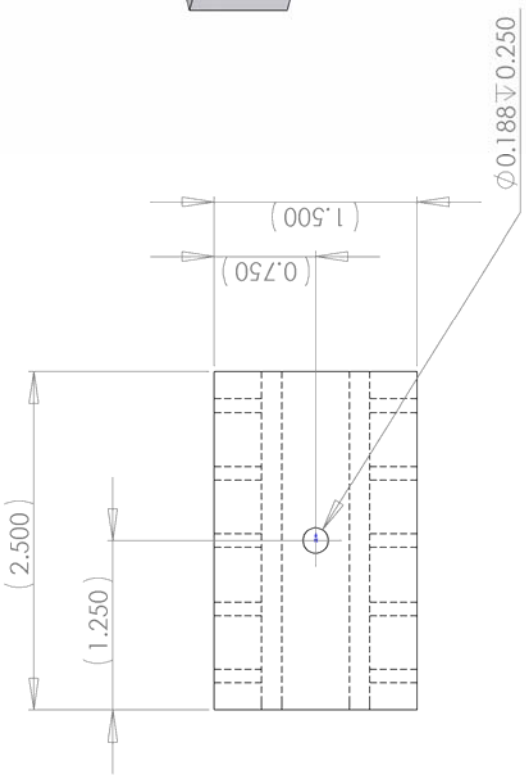
⌀0.188↧0.250
(1.500)
(0.750)
(2.500)
(1.250)

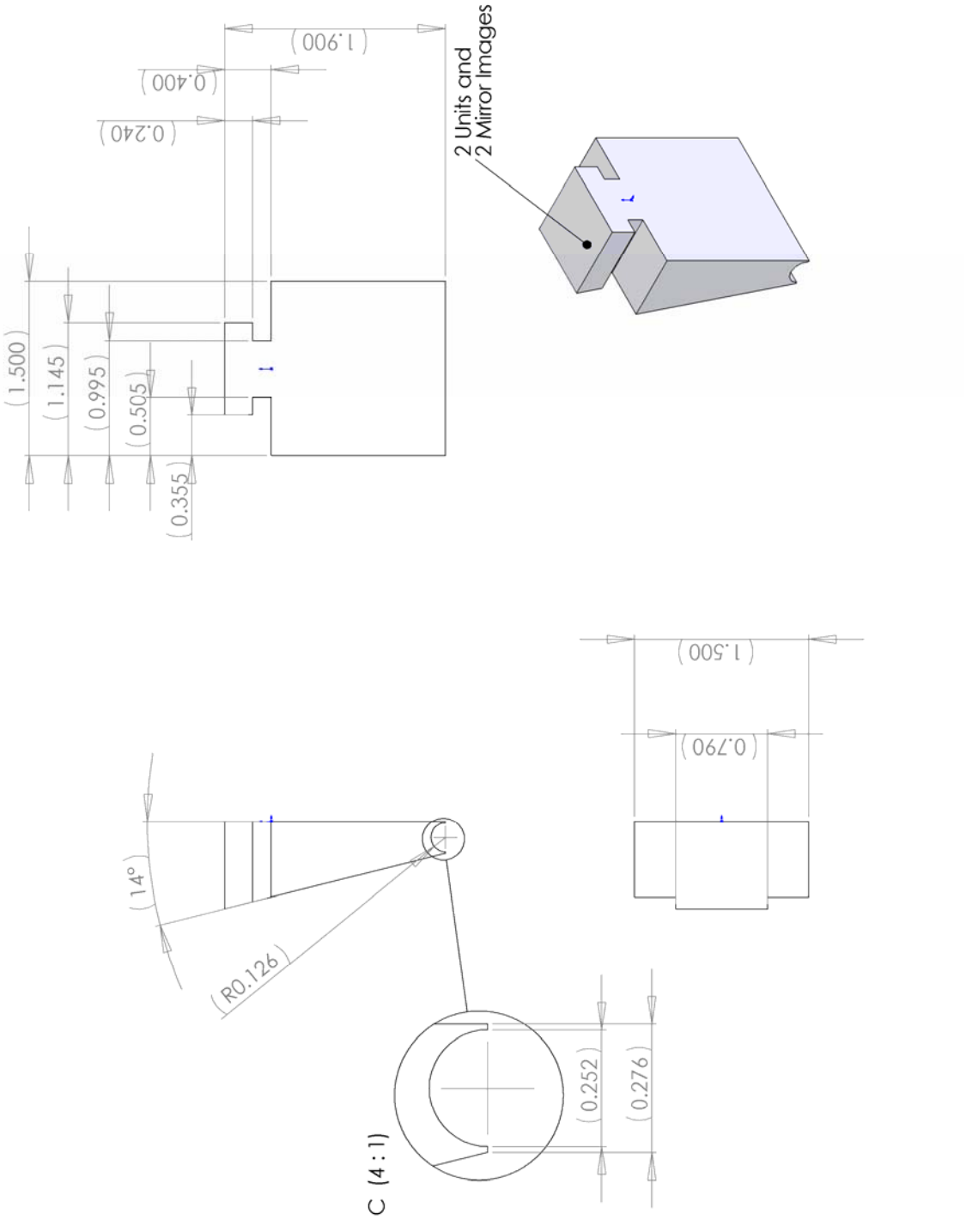
1.900
0.400
0.240
1.500
1.145
0.995
0.505
0.355
2 Units and
2 Mirror Images
1.500
0.790
14°
R0.126
0.252
0.276
C (4 : 1)

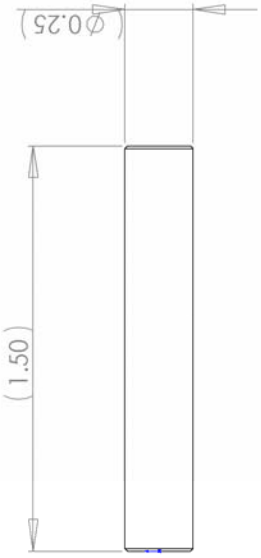
(Ø0.25)
(1.50)

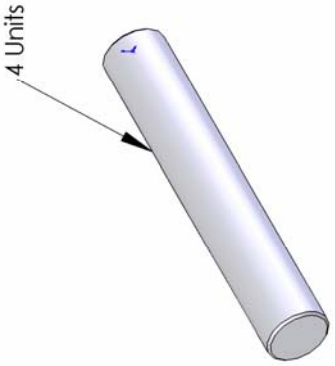
4 Units

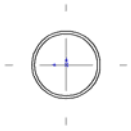

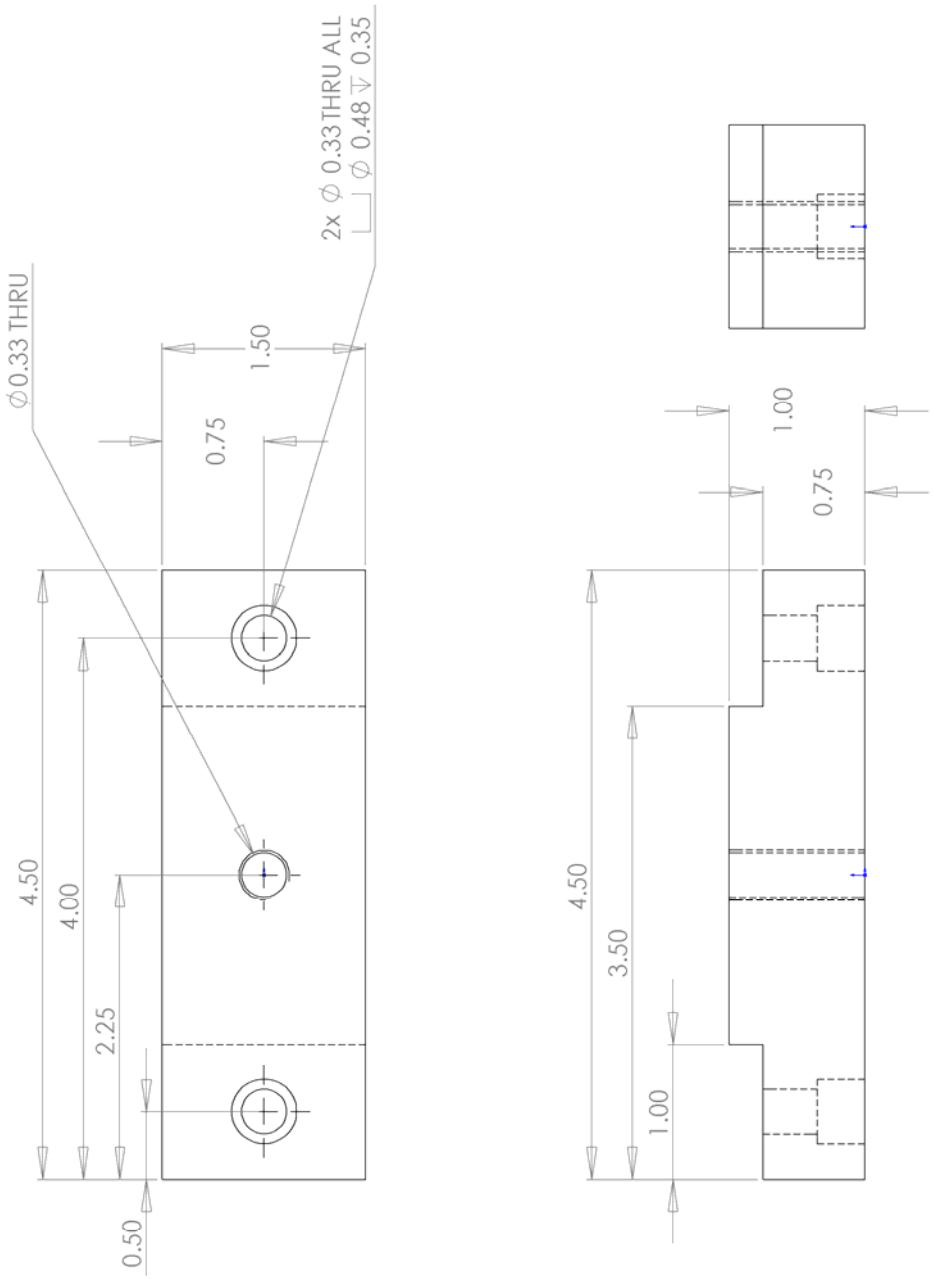
2x ⌀ 0.33 THRU ALL
⌴ ⌀ 0.48 ▽ 0.35
⌀0.33 THRU
1.50
0.75
4.50
4.00
2.25
0.50
1.00
0.75
4.50
3.50
1.00

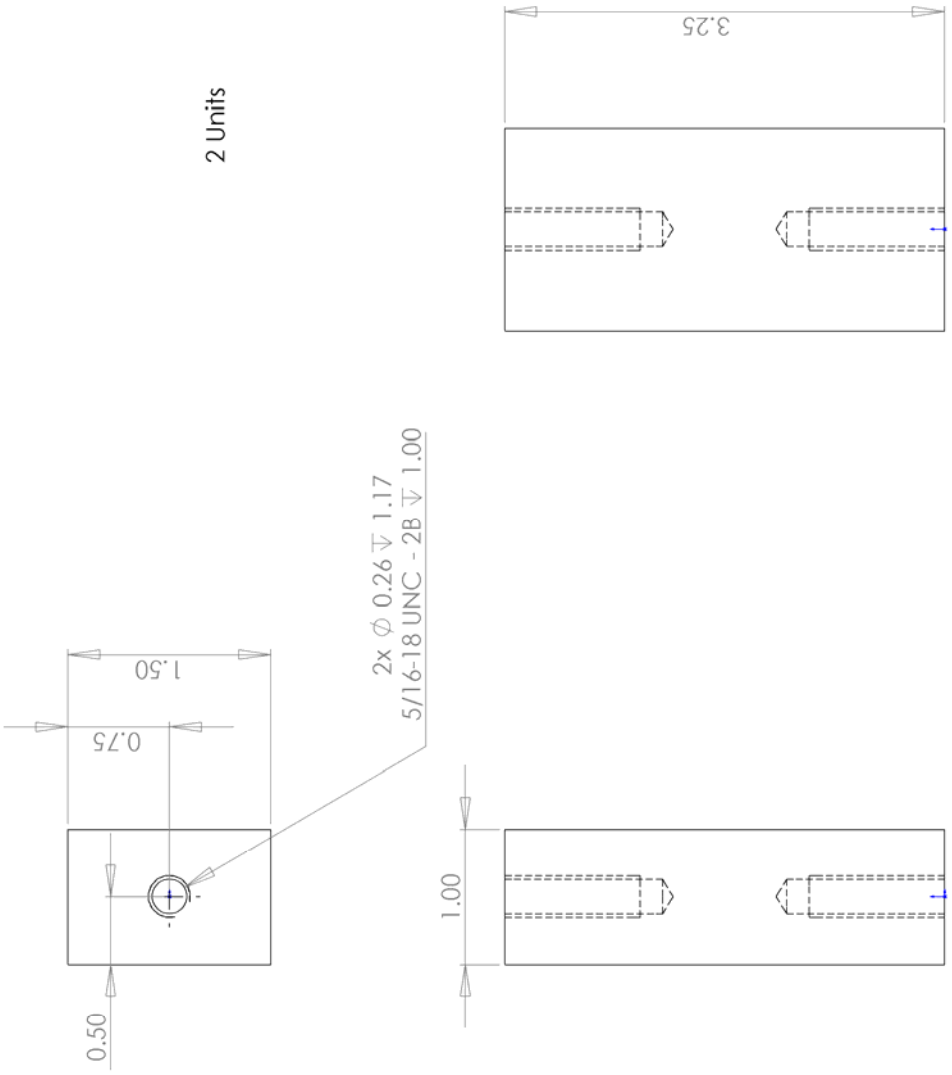
2 Units
3.25
2x ⌀ 0.26 ↧ 1.17
5/16-18 UNC - 2B ↧ 1.00
1.50
0.75
0.50
1.00

VITA

Name:	Daniel Osagie Oyinkuro Ayewah
Address:	Texas A&M University Department of Aerospace Engineering H.R. Bright Building, Rm. 701, Ross Street - TAMU 3141 College Station TX 77843-3141
Email Address:	dayewah@gmail.com
Education:	B.S., Aerospace Engineering, Texas A&M University, 2004 M.S., Aerospace Engineering, Texas A&M University, 2007